Argon offline-AMS source apportionment of organic aerosol over yearly cycles for an urban, rural and marine site in Northern Europe

C. Bozzetti[1], Y. Sosedova[1], M. Xiao[1], K. R. Daellenbach[1], V. Ulevicius[2], V. Dudoitis[2], G. Mordas[2], S. Byčenkienė[2], K. Plauškaitė[2], A. Vlachou[1], B. Golly[3], B. Chazeau[1], J.-L. Besombes[4], U. Baltensperger[1], J.-L. Jaffrezo[3], J. G. Slowik[1], El Haddad[1], I., and A. S. H. Prévôt[1]

[1] {Laboratory of Atmospheric Chemistry, Paul Scherrer Institute (PSI), 5232 Villigen-PSI, Switzerland}

[2] {Department of Environmental Research, SRI Center for Physical Sciences and Technology, LT-02300 Vilnius, Lithuania}

[3] {Université Grenoble Alpes, CNRS, LGGE, 38000 Grenoble, France}

[4] {Université Savoie Mont-Blanc, LCME, F-73000 Chambéry, France}

Correspondence to: A. S. H. Prévôt (andre.prevot@psi.ch); I. El Haddad (imad.el-haddad@psi.ch)

Abstract

The widespread use of Aerodyne aerosol mass spectrometers (AMS) has greatly improved real-time organic aerosol (OA) monitoring, providing mass spectra that contain sufficient information for source apportionment. However, AMS field deployments remain expensive and demanding, limiting the acquisition of long-term datasets at many sampling sites. The offline application of aerosol mass spectrometry entailing the analysis of nebulized water extracted filter samples (offline-AMS) increases the spatial coverage accessible to AMS measurements, being filters routinely collected at many stations worldwide.

PM_1 (particulate matter with an aerodynamic diameter <1 μm) filter samples were collected during an entire year in Lithuania at three different locations representative of three typical

environments of the South-East Baltic region: Vilnius (urban background), Rūgšteliškis (rural terrestrial), and Preila (rural coastal). Aqueous filter extracts were nebulized in Ar, yielding the first AMS measurements of water-soluble atmospheric organic aerosol (WSOA) without interference from air fragments. This enables direct measurement of the CO^+ fragment contribution, whose intensity is typically assumed to be equal to that of CO_2^+. Offline-AMS spectra reveal that the water soluble CO_2^+:CO^+ ratio not only shows values systematically >1 but is also dependent on season, with lower values in winter than in summer.

AMS WSOA spectra were analyzed using positive matrix factorization (PMF), which yielded 4 factors. These factors included biomass burning OA (BBOA), local OA (LOA) contributing significantly only in Vilnius, and two oxygenated OA (OOA) factors, summer OOA (S-OOA) and background OOA (B-OOA) distinguished by their seasonal variability. The contribution of traffic exhaust OA (TEOA) was not resolved by PMF due to both low concentrations and low water solubility. Therefore, the TEOA concentration was estimated using a chemical mass balance approach, based on the concentrations of hopanes, specific markers of traffic emissions. AMS-PMF source apportionment results were consistent with those obtained from PMF applied to marker concentrations (i.e. major inorganic ions, OC/EC, and organic markers including polycyclic aromatic hydrocarbons and their derivatives, hopanes, long-chain alkanes, monosaccharides, anhydrous sugars, and lignin fragmentation products). OA was the largest fraction of PM_1 and was dominated by BBOA during winter with an average concentration of 2 μg m^{-3} (53% of OA), while summer-OOA (S-OOA), probably related to biogenic emissions was the prevalent OA source during summer with an average concentration of 1.2 μg m^{-3} (45% of OA).

PMF ascribed a large part of the CO^+ explained variability (97%) to the OOA and BBOA factors. Accordingly we discuss a new CO^+ parameterization as a function of CO_2^+, and $C_2H_4O_2^+$ fragments, which were selected to describe the variability of the OOA and BBOA factors.

1 Introduction

Atmospheric aerosols affect climate (Lohmann et al., 2004, Schwarze et al., 2006), human health (Dockery et al., 2005, Laden et al., 2000), and ecosystems on a global scale. Quantification and characterization of the main aerosol sources are crucial for the development of effective mitigation strategies. The Aerodyne aerosol mass spectrometer (AMS, Canagaratna et al., 2007) and aerosol chemical speciation monitor (ACSM, Ng et al.,

2011, Fröhlich et al., 2013) have greatly improved air quality monitoring by providing real-time measurements of the non-refractory (NR) submicron aerosol (PM_1) components. Analysis of organic mass spectra using positive matrix factorization (PMF, Paatero, 1997; Paatero and Tapper, 1994) has enabled the quantitative separation of OA factors, which can be subsequently related to major aerosol sources and formation processes (e.g. Lanz et al., 2007; Lanz et al., 2010; Zhang et al., 2011; Ulbrich et al., 2009; Elser et al., 2016 a). Despite its numerous advantages, AMS field deployment remains expensive and demanding, and therefore most of the studies are typically restricted to short-time periods and a single (or few) sampling site(s). The limited amount of long-term datasets suitable for OA source apportionment severely limits model testing and validation (Aksoyoglu et al., 2011; Aksoyoglu et al., 2014; Baklanov et al., 2014), as well as for the development of appropriate pollution mitigation strategies. AMS analysis of aerosol filter samples (Lee et al., 2011; Sun et al., 2011; Mihara and Mochida, 2011; Daellenbach et al., 2016), which are routinely collected at many stations worldwide, broadens the temporal and spatial scales available for AMS measurements.

In this study we present the application of the offline-AMS methodology described by Daellenbach et al. (2016) to yearly cycles of filter samples collected in parallel at three different locations in Lithuania between September 2013 and August 2014. The methodology consists of water extraction of filter samples, followed by nebulization of the liquid extracts, and subsequent measurement of the generated aerosol by high-resolution time-of-flight AMS (HR-ToF AMS). In this work, organic aerosol water extracts were nebulized in Ar, permitting direct measurement of the CO^+ ion (Fig. S1), which is typically not directly quantified in AMS data analysis due to interference with N_2^+, but is instead estimated as being equal to CO_2^+ (Aiken et al., 2008). Direct measurement of CO_2^+ better captures the variability in the total OA mass and its elemental composition as well as potentially improving source apportionment of ambient aerosol. Aerosol elemental ratios and oxidation state are of particular relevance as they provide important constraints for understanding aerosol sources, processes, and for the development of predictive aerosol models (Canagaratna et al., 2015).

Aerosol composition in the south-east Baltic region has so far received little attention. To our knowledge the only investigation of OA sources in this area was during a five-day period of intense land clearing activity occurring in the neighboring Russian enclave of Kaliningrad (Ulevicius et al., 2016; Dudoitis et al., 2016), in which transported biomass burning emissions

dominated the aerosol loading. OA source contributions under less extreme conditions remain unstudied, with the most relevant measurements performed in Estonia with a mobile lab during March 2014 at two different locations (Elser et al., 2016b). On-road measurements revealed large traffic contributions with an increase of 20% from rural to urban environments. Also, residential biomass burning (BB) and oxygenated OA (OOA) contributions were found to be substantial.

In this study we present a complete source apportionment of the submicron OA fraction following the methodology described by Daellenbach et al. (2016) in order to quantify and characterize the main OA sources affecting the Lithuanian air quality. The three sampling stations were situated in the Vilnius suburb (urban background), Preila (rural coastal background), and Rūgšteliškis (rural terrestrial background), covering a wide geographical domain and providing a good overview of the most typical Lithuanian and south-eastern Baltic air quality conditions and environments. PMF analysis of offline-AMS measurements are compared with the results reported by Ulevicius et al. (2016) and with PMF analysis of chemical marker measurements obtained from the same filter samples.

2 Sampling and offline measurements

2.1 Site description and sample collection

We collected 24-h integrated PM_1 filter samples at 3 different stations in Lithuania from 30 September 2013 to 2 September 2014 using 3 High-Volume samplers (Digitel DHA80, and DH-77) operating at 500 L min^{-1}. In order to prevent large negative filter artifacts, the high volume were equipped with temperature control systems maintaining the filter storage temperature always below 25°C, which is lower or comparable to the maximum daily temperature during summer. The particulate matter was collected on 150-mm diameter quartz fiber filters (Pallflex Tissuquartz 2500QAT-UP / pure quartz, no binder) pre-baked at 800°C for 8 h. Filter samples were wrapped in pre-baked aluminum foils (400°C for 6 h), sealed in polyethylene bags and stored at -20°C after exposure. Field blanks were collected and stored following the same procedure.

Sampling was conducted at urban (Vilnius), rural terrestrial (Rūgšteliškis) and rural coastal (Preila) monitoring sites (Fig. 1). The rural terrestrial site of Rūgšteliškis serves as a baseline against which urban-specific sources in the major population center of Vilnius can be

compared. The rural coastal site of Preila provides an opportunity to distinguish terrestrial and marine sources.

The sampling station in Vilnius is located at the Center for Physical Sciences and Technology campus (54°38' N, 25°10' E, 165 m a.s.l.) 12 km southwest of the city center (population: 535000) and is classified as an urban background site. The site is relatively far from busy roads, and surrounded by forests to the north/northeast, and by a residential zone to the south/east. It is ca. 350 km distant from the Baltic coast, and 98 km from the Rūgšteliškis station (Fig. 1).

The station in Preila (55°55' N, 21°04' E, 5 m a.s.l.) is a representative rural coastal background site, situated in the Curonian Spit National Park on the isthmus separating the Baltic Sea from the Curonian Lagoon. The monitoring station is located <100 m from the Baltic shore. The closest populated area is the village of Preila (population: 200 inhabitants), located 2 km to the south.

The rural terrestrial station of Rūgšteliškis (55°26’ N and 26°04’ E, 170 m a.s.l.) is located in the eastern part of Lithuania, about 350 km from the Baltic Sea. The site is surrounded by forest and borders the Utenas Lake in the southwest. The nearest residential areas are Tauragnai, Utena (12 km and 26 km west of the station, population: 32000 inhabitants) and Ignalina (17 km southeast of the station, population: 6000 inhabitants).

2.2 Offline-AMS analysis

The term *offline-AMS* will be used herein to refer to the methodology described by Daellenbach et al. (2016) and summarized below. For each analyzed filter sample, four 16-mm diameter filter punches were subjected to ultrasonic extraction in 15 mL of ultrapure water (18.2 MΩ cm at 25°C, total organic carbon (TOC) < 3 ppb) for 20 min at 30°C.

The choice of water instead of an organic solvent is motivated by two arguments:

- Water yields the lowest background and hence the highest signal to noise compared to other highly pure solvents (including methanol, dichloromethane and ethyl acetate).
- In contrast to the water extraction, the use of organic solvents precludes the quantification of the organic content in the extracts (e.g. by using a total OC analyzer), which in turn prevents a quantitative source apportionment.

Liquid extracts were then filtered and atomized in Ar (≥99,998 % Vol. abs., Carbagas, CH-3073 Gümligen, Switzerland) using an Apex Q nebulizer (Elemental Scientific Inc., Omaha NE 68131 USA) operating at 60°C. The resulting aerosol was then dried by passing through a Nafion drier (Perma Pure, Toms River NJ 08755 USA), and subsequently analyzed by a HR-ToF-AMS. 12 mass spectra per filter sample were collected (AMS V-mode, *m*/*z* 12-232, 30 s collection time per spectrum). A measurement blank was recorded before and after each sample by nebulizing ultrapure water for 12 minutes. Field blanks were measured following the same extraction procedure as the collected filter samples, yielding a signal not statistically different from that of nebulized milliQ water. Finally we registered the AMS fragmentation spectrum of pure gaseous CO_2 (≥99,7 % Vol, Carbagas, CH-3073 Gümligen, Switzerland), in order to derive its CO_2^+:CO^+ ratio.

Offline-AMS analysis was performed on 177 filter samples in order to determine the bulk water-soluble organic matter (WSOM) mass spectral fingerprints. In total, 63 filters from Rūgšteliškis, 42 from Vilnius, and 71 from Preila were measured in Ar. The reader is referred to DeCarlo et al. (2006) for a thorough description of the AMS operating principles and calibration procedures.

HR-ToF-AMS analysis software SQUIRREL (SeQUential Igor data RetRiEvaL, D. Sueper, University of Colorado, Boulder, CO, USA) v.1.53G and PIKA (Peak Integration by Key Analysis) v.1.11L for IGOR Pro software package (Wavemetrics, Inc., Portland, OR, USA) were utilized to process and analyze the AMS data. HR analysis of the AMS mass spectra was performed in the *m/z* range 12-115.

2.3 Supporting measurements

Additional offline analyses were carried out in order to validate and corroborate the offline-AMS source apportionment results. This supporting dataset was also used as input for PM_1 source apportionment as discussed below. The complete list of the measurements performed can be found in Table 1 and Table S1. Briefly, major ions were measured by ion chromatography (IC; Jaffrezo et al., 1998); elemental and organic carbon (EC, OC) were quantified by thermal optical transmittance following the EUSAAR2 protocol (Cavalli et al., 2010); water-soluble OC (WSOC) was measured by water extraction followed by catalytic oxidation and non-dispersive infrared detection of CO_2 using a total organic carbon analyzer (Jaffrezo et al., 2005). Organic markers were determined by gas chromatography-mass

spectrometry (GC-MS; Golly et al., 2015); high performance liquid chromatography (HPLC) associated with a fluorescence detector (LC 240 Perkin Elmer) and HPLC-pulsed amperometric detection (PAD; Waked et al., 2014) for 67 composite samples. Composites were created merging two consecutive filter samples, but no measurements are available for Vilnius during summer. Measurements included 18 polycyclic aromatic hydrocarbons (PAHs), alkanes (C21-C40), 10 hopanes, 13 methoxyphenols, 13 methyl-PAHs (Me-PAHs), 6 sulfur-containing-PAHs (S-PAHs), 3 monosaccharide anhydrides, and 4 monosaccharides (including glucose, mannose, arabitol, and mannitol). In this work ion concentrations always refer to the IC measurements.

Table 1. Overview of supporting measurements. A complete list of measured compounds can be found in table S1.

Analytical Method	**Measured compounds**	**Filters measured**
IC (Jaffrezo et al., 1998)	Ions	All
Thermal optical transmittance using Sunset Lab Analyzer (Birch and Cary, 1996) using EUSAAR2 protocol (Cavalli et al., 2010)	EC/OC	All
TOC analyzer using persulphate oxidation at 100°C of the OM, followed by CO_2 quantification with a non-dispersive infrared spectrophotometer (Jaffrezo et al., 1998)	WSOC	All
HPLC associated with fluorescence detector (LC 240 Perkin Elmer) (Golly et al., 2015, Besombes et al., 2001)	PAHs (table S1)	67 composite samples
GC-MS (with and without derivatization step) (Golly et al., 2015)	S-PAHs, Me-PAHs, alkanes, hopanes, methoxyphenols, others	67 composite samples

HPLC-PAD, (Waked et al., 2014)	Anhydrous sugars, sugars alcohols, monosaccharides	67 composite samples
Chemiluminescence (Environnement S.A., Model AC31M)	NO_x	Online (Vilnius only)

In the following, subscripts *avg*, and *med* will denote average and median values, respectively.

3 Source apportionment

Positive matrix factorization (PMF, Paatero and Tapper, 1994) is a bilinear statistical model used to describe the variability of a multivariate dataset as the linear combination of a set of constant factor profiles and their corresponding time series, as shown in Eq. (1):

$$x_{i,j} = \sum_{z=1}^{p}(g_{i,z} \cdot f_{z,j}) + e_{i,j} \quad (1)$$

Here *x*, *g*, *f*, and *e* denote elements of data, factor time series, factor profiles and residual matrices, respectively, while subscripts *i*,*j* and *z* are indices for time, measured variables, and factor number. The value *p* represents the total number of factors chosen for the PMF solution. The PMF algorithm iteratively solves Eq. (1) by minimizing the objective function *Q*, defined in Eq. (2) Only non-negative $g_{i,z}$ and $f_{z,j}$ values are permitted:

$$Q = \sum_i \sum_j \left(\frac{e_{i,j}}{s_{i,j}}\right)^2 \quad (2)$$

Here the $s_{i,j}$ elements represent entries in the input error matrix.

In this work the PMF algorithm was run in the robust mode in order to dynamically downweigh the outliers. The PMF algorithm was solved using the multilinear engine-2 (ME-2) solver (Paatero, 1999), which enables an efficient exploration of the solution space by *a priori* constraining the $g_{i,z}$ or $f_{z,j}$ elements within a certain variability defined by the scalar *a* ($0 \leq a \leq 1$) such that the modelled $g_{i,z}$' and $f_{z,j}$' satisfy Eq. (3):

$$\frac{(1-a)f_{z,n}}{(1+a)f_{z,m}} \leq \frac{f_{z,n}'}{f_{z,m}'} \leq \frac{(1+a)f_{z,n}}{(1-a)f_{z,m}} \quad (3)$$

Here *n* and *m* are any two arbitrary columns (variables) in the normalized F matrix. The Source Finder toolkit (SoFi, Canonaco et al., 2013, v.4.9) for Igor Pro software package (Wavemetrics, Inc., Portland, OR, USA) was used to configure the ME-2 model and for post-analysis. PMF analysis was applied to two complementary datasets: (1) organic mass spectra from offline-AMS measurements for the apportionment of OM sources and (2) molecular markers for the apportionment of the measured PM_1 mass. These two analyses are discussed separately below.

3.1 Offline-AMS PMF

In the following section we describe the offline-AMS source apportionment implementation, optimization and uncertainty assessment. Briefly, we selected the number of PMF factors based on residual analyses and solution interpretability; subsequently we explored the rotational uncertainty of our source apportionment model and discarded suboptimal solutions providing insufficient correlation of factor time series with external tracers. The offline-AMS source apportionment returns the water soluble PMF factor concentrations. Daellenbach et al. (2016) determined factor specific recoveries (including PMF factor extraction efficiencies), by comparing offline-AMS and online-ACSM OA source apportionments. In particular, the filter samples were collected for one year during an online-ACSM monitoring campaign conducted at the same sampling station. Briefly, the factor recoveries were determined as the ratio between the water soluble OA PMF-factor concentrations retrieved from offline-AMS source apportionment divided by the OA PMF factor concentrations obtained from ACSM OA source apportionment. Factor specific recoveries and corresponding uncertainties were determined for HOA, BBOA, COA, and OOA. Applying these recoveries enabled scaling the water soluble factor concentrations to the corresponding bulk OA concentrations. A sensitivity analysis of these recoveries was reported in Section 3.1.3, and the corresponding uncertainty was propagated to the source apportionment results.

A second selection step was carried out on the rescaled solutions as described in section 3.1.3. The offline-AMS source apportionment results presented in this study represent the average of the retained rescaled PMF solutions, while their variability represents our best estimate of the source apportionment uncertainty.

3.1.1 Inputs

The offline-AMS input matrices include in total 177 filter samples (62 filters from Rūgšteliškis, 42 from Vilnius, and 73 from Preila). Each filter sample was represented on average by 12 mass spectral repetitions to explore the effect of AMS and nebulizer stability on PMF outputs. A corresponding measurement blank was subtracted from each mass spectrum. The input PMF matrices included 269 organic fragments fitted in the mass range (12-115). The input error $s_{i,j}$ elements include the blank variability ($\sigma_{i,j}$) and the uncertainty related to ion counting statistic and ion-to-ion signal variability at the detector ($\delta_{i,j}$, Allan et al., 2003; Ulbrich et al., 2009):

$$s_{i,j} = \sqrt{\delta_{i,j}^2 + \sigma_{i,j}^2} \quad (4)$$

We applied a minimum error to the $s_{i,j}$ matrix elements according to Ulbrich et al. (2009), and a down-weighting factor of 3 to all fragments with an average signal to noise lower than 2 (Ulbrich et al., 2009). Input data and error matrices were rescaled such that the sum of each row is equal to the estimated WSOM concentration, which is calculated as the product of the measured WSOC multiplied by the $OM:OC_i$ ratios determined from the offline-AMS PMF results.

3.1.2 Overview of retrieved factors and estimate of traffic exhaust OA (TEOA)

We used a 4-factor solution to represent the variability of the input data. The 4 separated OA factors included the following:

1/ a biomass burning OA (BBOA) factor highly correlated with levoglucosan originating from cellulose pyrolysis;

2/ a local OA (LOA) factor explaining a large fraction of N-containing fragments variability and contributing mostly in Vilnius during summer and spring;

3/ a background oxygenated-OA (B-OOA) factor showing relatively stable contributions at all seasons;

4/ a summer-OOA (S-OOA) factor showing increasing concentrations with the average daily temperature.

If the number of factors is decreased to 3, a mixed BBOA/B-OOA factor is retrieved, and significant structure appears in the residuals during winter (Fig. S2, S3, S4). Increasing the

number of factors to 5 and 6, leads to a splitting of OOA factors that cannot be interpreted in terms of specific aerosol sources/processes (Fig. S2, S3). The further separated OOA factor in the 5-factor solution possibly derived from the splitting of B-OOA; in fact the sum of the newly separated OOA and B-OOA in the 5-factor solution correlated well with the B-OOA time series from the 4-factor solution (R = 0.93). Overall, a clear structure removal in the residual time-series was observed until a number of factors equal to 4 (Fig. S4, S5).

We also explored a 5-factor solution in which a hydrocarbon-like OA (HOA) profile from Mohr et al. (2012) was constrained to estimate the TEOA contribution. However, the water-soluble TEOA (WSTEOA) contribution to WSOM was estimated as 0.2%$_{avg}$ (section 3.1.4), likely too small for PMF to resolve. We performed 100 PMF runs by randomly varying the HOA a-value. The obtained results showed a low TEOA correlation with hopanes (R_{max} = 0.25, R_{min} = -0.15) with 45% of the PMF runs associated with negative Pearson correlation coefficients, supporting the hypothesis that this factor has too small contribution in the water extracts to be resolved. Therefore, we selected the 4-factor solution as our best representation of the data, while TEOA was instead estimated by a chemical mass balance (CMB) approach and not based on AMS mass spectral features.

TEOA concentrations are estimated using a CMB approach that assumes hopanes, present in lubricant oils engines, (Subramanian et al., 2006) to be unique tracers for traffic. However, hopanes can also be emitted upon combustion of different types of fossil fuel, in particular by coal combustion (Rutter et al., 2009), therefore the traffic contribution estimated here, although very small (as discussed in the result section) should be considered as an upper estimate. Still, the EC/hopanes ratio determined in this work (900±100) is consistent with EC/hopanes for TE (1400±900: He et al., 2006; He et al., 2008; El Haddad et al., 2009; Fraser et al., 1998) and not with the coal EC/hopanes from literature profiles (300±200: Huang et al., 2014; supplementary information (SI)). To assess the traffic exhaust OC (TEOC) contribution we used the sum of the four most abundant hopanes (17a(H),21b(H)-norhopane, 17a(H),21b(H)-hopane, 22S,17a(H),21b(H)-homohopane, and 22R,17a(H),21b(H)-homohopane (hopanes$_{sum}$)). The TEOC contribution was estimated from the average hopanes$_{sum}$/TEOC ratio (0.0012±0.0005) from tunnel measurements reported by He et al. (2006), He et al. (2008), El Haddad et al. (2009), and Fraser et al. (1998), where the four aforementioned hopanes were also the most abundant. In order to rescale TEOC to the total TEOA concentration we assumed an OM:OC$_{TEOA}$ ratio of 1.2±0.1 (Aiken et al., 2008, Mohr

et al., 2012, Docherty et al., 2011, Setyan et al., 2012). The uncertainty of the estimated TEOA concentration was assessed by propagating the uncertainties relative to the $OM:OC_{TEOA}$ ratio (8.3%), the $hopanes_{sum}$/TEOC ratio (41.7%), the hopane measurement repeatability (11.5%), and detection limits (7 pg m^{-3}).

3.1.3. Source apportionment uncertainty

A common issue in PMF is the exploration of the rotational ambiguity, here addressed by performing 100 PMF runs initiated using different input matrices. We adopted a bootstrap approach (Davison and Hinkley, 1997) to generate the new input data and error matrices (Brown et al., 2015). Briefly, the bootstrap algorithm generates new input matrices by randomly resampling mass spectra from the original input matrices. As already mentioned, the input matrices contained ca. 12 mass spectral repetitions per filter sample; therefore the bootstrap approach was implemented in order to resample random filter sample mass spectra together with the corresponding measurement repetitions. Each newly generated PMF input matrix had a total number of samples equal to the original matrices (177 samples), although some of the original 177 filter samples are represented several times, while others are not represented at all. Overall we resampled on average 63±2% of the filter samples per bootstrap run. The generated data matrices were finally perturbed by varying each $x_{i,j}$ element within twice the corresponding uncertainty ($s_{i,j}$) assuming a normal distribution of the errors. Solutions were selected and retained according to three acceptance criteria based on PMF factor correlations with corresponding tracers: BBOA vs. levoglucosan, B-OOA vs. NH_4^+, and S-OOA vs. average daily temperature. In order to discard suboptimal PMF runs, we only retained solutions associated with positive Pearson correlation coefficients for each criterion, for both the individual stations and the entire dataset. In total 95% of the solutions were retained following this approach. We note that no solution was discarded based on the first two criteria.

The offline-AMS PMF analysis provides the water-soluble contribution of the identified aerosol sources. In order to rescale the water-soluble organic carbon concentration of a generic factor *z* (WSZOC) to its total OC concentration (ZOC) we used the factor recoveries (R_Z) determined by Daellenbach et al. (2016) according to Eq. (5):

$$ZOC_i = \frac{WSZOC_i}{R_z} \quad (5)$$

For each PMF factor (BBOA, W-OOA, and S-OOA), the water-soluble organic carbon contribution was determined from the OM:OC ratio calculated from the (water-soluble) factor mass spectrum (Aiken et al. 2008). For LOA, whose recovery was not previously reported, R_{LOA} was estimated from a single parameter fit according to Eq. (6)

$$OC = TEOC + \frac{WSBBOA}{(OM/OC)_{WSBBOA} \cdot R_{BBOA}} + \frac{WSW-OOA}{(OM/OC)_{WSS-OOA} \cdot R_{OOA}} + \frac{WSS-OOA}{(OM/OC)_{WSB-OOA} \cdot R_{OOA}} + \frac{WSLOA}{(OM/OC)_{LOA} \cdot \boldsymbol{R_{LOA}}} \quad (6)$$

Here the water-soluble OA factor concentrations were converted to the corresponding water-soluble OC concentrations to fit the measured OC. For each of the 95 retained PMF solutions, Eq. (6) was fitted 100 times by randomly selecting a set of 100 R_{BBOA}, R_{OOA} value combinations from those determined by Daellenbach et al. (2016). Each fit was initiated by perturbing the input OC_i and $TEOC_i$ within their uncertainties, assuming a normal distribution of the errors. Additionally, in order to explore the effect of possible bulk extraction efficiency (WSOC/OC) systematic measurement biases on our R_Z estimates, we also perturbed the OC, WSOC (Daellenbach et al., 2016) inputs. Specifically, we assumed an estimated accuracy bias of 5% for each of the perturbed parameters, which corresponds to the OC and WSOC measurement accuracy. In a similar way, we also perturbed the input R_{BBOA} and R_{OOA} assuming an accuracy estimate of 5% deriving from a possible OC measurement bias in Daellenbach et al. (2016) which could have affected the R_Z determination. In total $9.5 \cdot 10^3$ fits were performed (Eq. 6) and we retained only solutions (and corresponding perturbed R_Z combinations) associated with average OC residuals not statistically different from 0 within 1σ for each station individually and for summer and winter individually (~8% of the $9.5 \cdot 10^3$ fits, Fig. S6). The OC residuals of the accepted solutions did not manifest a clear correlation with the LOA concentration (Fig. S7), indicating that the estimated R_{LOA} was properly fitted, without compensating for unexplained variability of the PMF model or biases from the other R_z. Fig. S8 shows the probability density functions (PDF) of the retained perturbed R_z which account for all uncertainties and biases mentioned above. $R_{LOA,med}$ was estimated to be equal to 0.66 (1st quartile 0.61, 3rd quartile 0.69, Fig. S8), while the retained R_{BBOA} and R_{OOA} values ($R_{BBOA,med}$ 0.57, 1st quartile 0.55, 3rd quartile 0.60; $R_{OOA,med}$ 0.84, 1st quartile 0.81, 3rd quartile 0.88) were systematically lower than those reported by Daellenbach et al. (2016), reflecting the lower bulk extraction efficiency (bulk EE = WSOC/OC) measured for this dataset (median = 0.59, 1st quartile = 0.51, 3rd quartile = 0.72 *vs.* median = 0.74, 1st quartile = 0.66, 3rd quartile 0.90 in Daellenbach et al. (2016)). All the retained R_k combinations are available at DOI: doi.org/10.5905/ethz-1007-53.

Source apportionment uncertainties ($\sigma_{S.A.}$) were estimated for each sample *i* and factor *z* as the standard deviation of all the retained PMF solutions (~8% of the $9.5 \cdot 10^3$ fits). In addition to the rotational ambiguity of the PMF model (explored by the bootstrap technique) and R_Z uncertainty, each PMF solution included on average 10 repetitions for each filter sample, and hence $\sigma_{S.A.}$ accounted also for measurement repeatability. In this work, the statistical significance of a factor contribution is calculated based on $\sigma_{S.A.,z,i}$ (Tables S2 and S3).

In general the recovery estimates reported in Daellenbach et al. (2016) represent the most accurate estimates available, being constrained to match the online-ACSM source apportionment results. The R_Z combinations reported by Daellenbach et al. (2016) demonstrated to positively apply to this dataset, enabling properly fitting the measured Bulk EE (WSOC/OC) with unbiased residuals and therefore providing a further confidence on their applicability (we note that in Eq. 6 we fitted OC as function of $1/R_Z$ and $WSOC_{Z,i}$, therefore R_Z fitted WSOC/OC = Bulk EE). In general further R_Z determinations calculated comparing offline-AMS and online-AMS source apportionments would be desirable in order to provide more robust R_Z estimates. In absence of a-priori R_Z values for specific factors (e.g. for LOA in this study) we recommend constraining the R_Z combinations reported by Daellenbach et al. (2016) as a-priori information to fit the unknown recoveries, with the caveat that the R_Z combinations reported by Deallenbach et al. (2016) were determined for filter samples extracted with water following a specific procedure; therefore we recommend adopting these R_Z combinations for filter samples extracted in the same conditions. Nevertheless the R_Z combinations reported by Daellenbach et al. (2016) should be tested also for filters water extracted in different conditions to verify whether they can properly fit the Bulk EE. In case the R_Z combinations reported by Daellenbach et al. (2016) would not apply for a specific location or extraction procedure (i.e. not enabling a proper fit of Bulk EE) we recommend a R_Z redetermination by comparing the offline-AMS source apportionment results with well-established source apportionment techniques. In absence of data to perform a well-established source apportionment, we recommend to fit all the R_Z to match the bulk EE (i.e. fitting all the recoveries similarly as in Eq. 6 without constraining any a-priory R_Z value).

In general, the offline-AMS technique assesses less precisely the contribution of the lower water soluble factors. The higher uncertainty mostly stems from the larger PMF rotational ambiguity when separating a factor characterized by low concentration in the aqueous filter extracts. Nevertheless, the uncertainty is dataset dependent, as the separation of source

components with low water solubility can be improved in case of distinct time variability characterizing those sources in comparison with the other aerosol sources. The low aqueous concentration of scarcely water soluble sources in fact can be partially overcome by the large signal/noise characterizing the offline-AMS technique (170 on average for this dataset).

3.1.4. Sensitivity of PMF to the un-apportioned TEOA fraction

Despite representing only a small fraction, the un-apportioned water-soluble TEOA (WSTEOA) contribution could in theory affect the apportionment of the other sources in the PMF model. To assess this, we performed a PMF sensitivity analysis by subtracting the estimated WSTEOA concentration from the input PMF data matrix, and by propagating the estimated WSTEOA uncertainty (section 3.1.2) in the input error matrices. To estimate the WSTEOA concentration we assumed R_{TEOA} of 0.11±0.01 (Daellenbach et al., 2016) and we used the HOA profile reported by Mohr et al. (2012) as surrogate for the TEOA mass spectral fingerprint. This approach is equivalent to constraining both the WSTEOA time series and factor profile. Overall the WSTEOA contribution to WSOM was estimated as $0.2\%_{avg}$, making a successful retrieval of WSTEOA unlikely (Ulbrich et al., 2009). Consistently, PMF results obtained from this sensitivity analysis indicated that BBOA and B-OOA were robust, showing only 1% difference from the average offline-AMS source apportionment results, with BBOA increased and B-OOA decreased. S-OOA and LOA instead showed larger deviations from the average source apportionment results (S-OOA increased by 8% and LOA decreased by 15%), yet within our source apportionment uncertainties. These results highlight the marginal influence of the un-apportioned WSTEOA fraction on the other factors.

3.2 Marker-PMF: measured PM_1 source apportionment

In the following section we describe the implementation of source apportionment using chemical markers (marker-PMF), as well as its optimization and uncertainty assessment. We discuss the number of factors and the selection of specific constraints to improve the source separation. Subsequently we discuss the source apportionment rotational uncertainty, and the sensitivity of our PMF results to the number of source specific markers, and to the assumed constraints.

3.2.1 Inputs

The marker-PMF yields a source apportionment of the entire measured PM_1 fraction (organic and inorganic). Measured PM_1 is defined here as the sum of EC, ions measured via IC, and OM estimated from OC measurements multiplied by the $(OM:OC)_i$ ratio determined from the offline-AMS PMF results by summing the factor profiles OM:OC ratios weighted by the time dependent factor relative contributions (rescaled by the recoveries). PMF was used to analyze a data matrix consisting of selected organic molecular markers, ions measured by IC, EC, and the remaining OM fraction (OM_{res}) calculated as the difference between OM and the sum of the organic markers already included in the input matrix. OM_{res} represented on average 95±2% of total OM. The marker-PMF analysis is limited by the lack of elemental measurements (e.g. metals and other trace elements) typically used to identify mineral dust and certain anthropogenic sources. All markers showing concentrations above the detection limits for more than 25% of the samples were selected as input variables (72 in total). The PMF input matrices contain 67 composite samples (31 for Rūgšteliškis, 29 for Preila, and 7 for Vilnius). The errors ($s_{i,j}$) were estimated by propagating for each j variable the detection limits (DL) and the relative repeatability (RR) multiplied by the $x_{i,j}$ concentration according to Eq. (7) (Rocke and Lorenzato, 1995):

$$s_{i,j}=\sqrt{(DL_j{}^2+(x_{i,j}\cdot RR_{i,j})^2)} \quad (7)$$

3.2.2 Number of factors and constraints

We selected a 7-factor solution to explain the variability of the measured PM_1 components. The retrieved factors were biomass burning (BB), traffic exhaust (TE), primary biological organic aerosol (PBOA), SO_4^{2-}-related secondary aerosol (SA), NO_3^--related SA, methane sulfonic acid (MSA)-related SA, and a Na^+-rich factor explaining the variability of inorganic components typically related to resuspension of mineral dust, sea salt, and road salt.

We first tested an unconstrained source apportionment. This led to a suboptimal separation of the aerosol sources, with large mixings of PMF factors associated with contributions of markers originating from different sources. In particular we observed mixing of BB markers (e.g. levoglucosan) with fossil fuel combustion markers such as hopanes, as well as with inorganic ions such as NO_3^- and Ca^{2+}. All these markers, although related to different emission/formation processes, are characterized by similar seasonal trends, i.e. higher

concentrations during winter than in summer. Specifically, the BB tracers increase during winter because of domestic heating activity, hopanes presumably because of the accumulation in a shallower boundary layer and lower photochemical degradation, NO_3^- because of the partitioning into the particle phase at low temperatures, and Ca^{2+} because winter was the windiest season and therefore was associated with the most intense resuspension.

We subsequently exploited the markers' source-specificity to set constraints for the profiles output by our model: for each individual source, we treated the contribution of the unrelated source-specific markers as negligible (e.g. we assumed that TE, SA, Na-rich factor and PBOA do not contribute to levoglucosan). In contrast, the non-source specific variables (EC, OM_{res}, (Me-)PAHs, S-PAHs, inorganic ions, oxalate, alkanes) were freely apportioned by the PMF algorithm. In a similar way we set constraints for primary markers (e.g. K^+ and Ca^{2+}) and combustion related markers (e.g. PAHs), which are not source-specific but the contribution of which can be considered as negligible in the SA factors. In this case the algorithm can freely apportion these markers to all the primary factors and combustion-related factors, respectively.

In details, EC, PAHs, and methyl-PAHs were constrained to zero in non-combustion sources, i.e. all profiles but TE and BB. While EC could partially derive from dust resuspension, literature profiles for this source suggest an EC contribution below 1% (Chow et al., 2003). This is expected to be also the case here given the distance of the three stations from residential areas and busy roads. Methoxyphenols and sugar anhydrides, considered to be unique BB markers, were constrained to zero in all sources but BB. Similarly, hopanes were constrained to zero in all factors but TE. We also assumed no contribution from glucose, arabitol, mannitol, and sorbitol to all secondary factors, and traffic exhaust. The SO_4^{2-} contribution from primary traffic emissions was estimated to be negligible, given the use of desulfurized fuel for vehicles in Lithuania. Likewise, alkane contributions were assumed to be zero in the SA factors, similar to the contribution of Ca^{2+}, Na^+, K^+ and Mg^{2+} in the SA factors and TE.

The number of factors was increased until no mixing between source-specific markers for different aerosol sources/processes was observed any more. Secondary sources instead were explained by three factors because of the distinct seasonal and site-to-site variability of MSA, NO_3^- and SO_4^{2-}. Oxalate correlated well with NH_4^+ (R=0.62) and the latter well with the sum of SO_4^{2-} and NO_3^- equivalents (R=0.98). Note that the aforementioned secondary tracers were

not constrained in any factor with the exception of SO_4^{2-} contributions which were assumed to be negligible in the TE factor. Moreover the 7-factor solution showed unbiased residuals (residual distribution centered at 0 within 1σ) for all the stations together and for each station individually, while lower order solutions showed biased residuals for at least one station or all the stations together.

PMF results obtained assuming only the aforementioned constraints returned suboptimal apportionments of OM_{res} and Na^+ between the BB and the Na^+-rich factor, with unusually high OM_{res} fractional contributions in the Na^+-rich factor and unusually high Na^+ contributions in the BB profile in comparison with literature profiles (Chow et al., 2003; Huang et al., 2014 and references therein; Schauer et al., 2001). Similarly the EC/OM_{res} value for TE was substantially lower than literature profiles (El Haddad et al., 2013 and references therein). Other constraints were therefore introduced to improve the separation of these three variables. Specifically, EC and OM_{res} were constrained in the traffic profile to be equal to 0.45 and 0.27 (*a*-value = 0.5) according to El Haddad et al. (2013), while EC:BB ratio was constrained to 0.1 (*a*-value = 1) according to Huang et al. (2014) and references therein. Na^+ was constrained to 0.2% (*a*-value = 1) in BB according to Schauer et al. (2001), while OM_{res} was constrained to zero in the Na^+-rich factor to avoid mixing with BB. Although this represents a strict constraint, we preferred avoiding constraining OM_{res} to a specific value for the Na^+-rich factor which could not be linked to a unique source but possibly represents different resuspension-related sources (e.g. sea salt, mineral dust and road dust). However, we expect none of the aforementioned sources to explain a large fraction of the submicron OM_{res} (the OC:dust ratio for dust profiles is 1-15% according to Chow et al., 2003). The sensitivity of our source apportionment to the constraints listed in this section is discussed in the next section.

3.2.3. Source apportionment uncertainty and sensitivity analyses

We explored the model rotational uncertainty by performing 20 bootstrap PMF runs, and by perturbing each input $x_{i,j}$ element within $2 \cdot s_{i,j}$ assuming a normal distribution of the errors. Results and uncertainties of the PMF model reported in this paper represent the average and the standard deviation of the bootstrap runs.

As discussed in section 3.2.2, we assumed the contribution of specific markers to be 0 in different factor profiles. Such assumptions preclude the PMF model to vary the contributions of these variables from 0 (Eq. 3). In order to explore the effect of such assumptions on our PMF results we loosened all these constraints assuming variable contributions equal to 50%, 37.5%, 25%, and 12.5% of their average relative contribution to measured PM_1. In all cases the *a*-value was set to 1. The average factor concentrations for the 12.5% case and the fully constrained average bootstrap PMF solutions were not statistically different (confidence interval of 95%, Fig. S9). Statistically significant differences arose for the of the SO_4^{2-}-related SA in the 50% and 37.5% cases, and the Na^+-rich factor in the 25% and 37.5% cases, indicating that loosening the constraints allowed additional rotational uncertainty in comparison to the uncertainty explored by the bootstrap approach. By contrast, the factors associated with large relative uncertainties from the marker source apportionment (TE and PBOA, Table S3) showed the best agreement in terms of concentrations (Fig. S9) with the fully constrained solution, suggesting that the variability introduced by loosening the constraints did not exceed that already accounted for by the bootstrap approach. As previously mentioned, the largest contribution discrepancies were observed for the SO_4^{2-}-related SA and Na^+-rich factor. Looser constraints increased the explained variability of primary components such as EC, arabitol, sorbitol, K^+, Mg^{2+}, and Ca^{2+} by the (secondary) SO_4^{2-}-related SA factor. The Na^+-rich factor showed increasing contributions from OM_{res} and from BB components such as methoxyphenols, and anhydrous sugars, which exhibited similar seasonal trends as the Na^+-rich factor. None of the marker-PMF factors showed statistically different average contributions (confidence interval of 95%) when tolerating a variability of the constrained variables within 12.5% of their relative contribution to PM_1. Note that with this degree of tolerance the contribution of OM to the Na^+-rich was 28%, which is unrealistically high compared to typically reported values for OM:dust ratios (<15% Chow et al., 2003). Therefore, we consider the fully constrained PMF solution to represent best the average composition of the contributing sources.

The marker-PMF source apportionment depends strongly on the input variables (i.e. measured markers), as these are assumed to be highly source specific. That is, minor sources, such as MSA-related SA and PBOA, are separated because source-specific markers were used as model inputs. Meanwhile, more variables were used as tracers for TE and BB (methoxyphenols (5 variables), sugar anhydrides (3 variables), and hopanes (5 variables)), which gives more weight to these specific sources. We explored the sensitivity of the PMF

results to the number and the choice of traffic and wood burning markers, by replacing them with randomly selected input variables. In total 20 runs were performed and the average contribution of the different sources to OM_{res} was compared with the marker source apportionment average results, where bootstrap was applied to resample time points. Results displayed in Fig. S10 are in agreement the apportionment of OM_{res} from BB within $11\%_{avg}$, highlighting its robustness. The agreement for TE was lower, which is not surprising given the lower contribution of this source and the smaller number of specific markers (hopanes). However, these uncertainties were within the marker source apportionment uncertainty (Fig. S10), implying that the results were not significantly sensitive to the number and the choice of input markers for BB and traffic exhaust.

4 Results and Discussion

4.1 PM_1 composition

An overview of the measured PM_1 composition can be found in Fig. 1. Measured PM_1 average concentrations were in general low, with lower values detected at the rural terrestrial site of Rūgšteliškis (5.4 $\mu g\ m^{-3}{}_{avg}$) than in Vilnius (6.7 $\mu g\ m^{-3}{}_{avg}$) and Preila (7.0 $\mu g\ m^{-3}{}_{avg}$). OM represented the major fraction of measured PM_1 for all seasons and stations, with $57\%_{avg}$ of the mass. The average OM concentrations were higher during winter (4.2 $\mu g\ m^{-3}$) than in summer (3.0 $\mu g\ m^{-3}$) at all sites probably to a combination of domestic wood burning activity and accumulation of the emissions in a shallower boundary layer. For similar reasons, EC average concentrations showed higher values during winter (0.42 $\mu g\ m^{-3}$) than in summer (0.25 $\mu g\ m^{-3}$). During summer, the average EC concentration was ~5 times higher in Vilnius (0.54 $\mu g\ m^{-3}$) than in Preila and Rūgšteliškis (0.12 and 0.11 $\mu g\ m^{-3}$, respectively), indicating an enhanced contribution from combustion emissions. In the absence of domestic heating during this period, a great part of these emissions may be related to traffic. During winter, EC concentrations were comparable at all sites (only 25% higher in Vilnius than in Preila and Rūgšteliškis). This suggests that a great share of wintertime EC may be related to BB, the average contribution of which is significant at all stations within 3σ (table S2). It should be noted that the highest measured PM_1 concentrations were detected at the remote rural coastal site of Preila during three different pollution episodes. In particular, the early March episode corresponded to the period analyzed by Ulevicius et al. (2016) and Dudoitis et al. (2016), and

was attributed to regional transport of polluted air masses associated to an intense land clearing activity characterized by large scale grass burning in the neighboring Kaliningrad region. SO_4^{2-} represented the second major component of measured PM_1 ($20\%_{med}$) at all sites and seasons. Its average concentration remained rather constant with only slightly higher concentrations in summer than in winter (1.2±0.7 μg m^{-3}, and 1.1±0.6 μg m^{-3} respectively). Overall SO_4^{2-} concentrations did not show large differences from site-to-site, suggestive of regional sources. By contrast NO_3^- showed a clear seasonality with larger contributions in winter (average 0.9±0.8 μg m^{-3} equivalent to 12% of measured PM_1) than in summer (0.03±0.03 μg m^{-3}), as expected from its semi-volatile nature.

4.2 OM source apportionment (Offline-AMS PMF)

The apportioned PMF factors were associated to aerosol sources/processes according to their mass spectral features, seasonal contributions and correlations with tracers. The four identified factors were BBOA, LOA, B-OOA, and S-OOA, which are thoroughly discussed below. The TEOA contributions instead were determined using a CMB approach.

BBOA was identified by its mass spectral features, with high contributions of $C_2H_4O_2^+$, and $C_3H_5O_2^+$ (Fig. 2), typically associated with levoglucosan fragmentation from cellulose pyrolysis (Alfarra et al., 2007), accordingly the BBOA factor time series correlated well with levoglucosan (Pearson correlation coefficient: R=0.90, Fig. S11). BBOA contributions were higher during winter and lower during summer (Fig. 3a). We determined the biomass burning organic carbon (BBOC) concentration from the BBOA time series divided by the $OM:OC_{BBOA}$ ratio determined from the corresponding HR spectrum. The winter levoglucosan/BBOC ratio was 0.16_{med}, consistent with values reported in continental Europe for ambient BBOC profiles (levoglucosan/BBOC range: 0.10-0.21, Zotter et al., 2014; Minguillón et al., 2011; Herich et al., 2014).

The second factor was defined as LOA because of its statistically significant contribution (within 3σ) only in Vilnius during summer (table S2), in contrast to other potentially local primary (e.g. BBOA) and secondary (S-OOA) sources which contributed at all sites. The LOA mass spectrum was characterized by a high contribution of N-containing fragments (especially $C_5H_{12}N^+$, and $C_3H_8N^+$), with the highest N:C ratio (0.049) among the apportioned PMF factors (0.029 for BBOA, 0.013 for S-OOA, 0.023 for B-OOA). A similar factor was also observed by Byčenkienė et al. (2016) using an ACSM at the same station. In that work,

high LOA concentrations were associated with wind directions from N-NW, and the authors suggested the sludge utilization system of Vilnius (UAB Vilniausvandenys) situated 3.9 km NW from the sampling station as a probable source.

Two different OOA sources (S-OOA and B-OOA) were resolved and exhibited different seasonal trends. Separation and classification of OOA sources from offline-AMS is typically different from that of online AMS and ACSM measurements, mainly due to the different time resolution. Few online-AMS studies reported the separation of isoprene-related OA factor (Budisulistiorini et al., 2013; Hu et al., 2015, Xu et al., 2015) mostly driven by isoprene epoxides chemistry. Xu et al. (2015) showed that nighttime monoterpene oxidation by nitrate radical contributes to less-oxidized OOA. However, the large majority of online-AMS OOA factors are commonly classified based on their volatility (semi-volatile OOA and low-volatility OOA) rather than on their sources and formation mechanisms.

This differentiation is typically achieved only for summer datasets when the temperature gradient between day and night is sufficiently high, yielding a detectable daily partitioning cycle of the semi-volatile organic compounds and NO_3^- between the gas and the particle phases. Online AMS datasets have higher time resolution than filter sampling, but sampling periods typically cover only a few weeks. Therefore the apportionment is driven by daily variability rather than seasonal differences. By contrast, in the offline-AMS source apportionment, given the 24-h time resolution of the filter sampling and the yearly cycle time coverage, the separation of the factors is driven by the seasonal variability of the sources and by the site-to-site differences. Therefore, the offline-AMS source apportionment separates factors by seasonal trends rather than volatility.

The resolved B-OOA factor explained a higher fraction than S-OOA. It was associated with background oxygenated aerosols as no systematic seasonal pattern was observed. However, B-OOA correlated well with NH_4^+ (R=0.69, Fig. S11), and had the highest OM:OC ratio among the apportioned PMF factors (2.21).

Unlike B-OOA, S-OOA showed a clear seasonality with higher contributions during summer, increasing exponentially with the average daily temperature (Fig. S12a). During summer the site-to-site S-OOA concentrations were not statistically different within a confidence interval of 95%, while during winter the site-to-site agreement was lower, possibly due to the larger model uncertainty associated with the low S-OOA concentrations. A similar S-OOA *vs.* temperature relationship was reported by Leaitch et al. (2011) for a terpene dominated

Canadian forest using an ACSM and by Daellenbach et al. (2016) and Bozzetti et al. (2016) for the case of Switzerland (Fig. S12b), using a similar source apportionment model. This increase in S-OOA concentration with temperature is consistent with the exponential increase in biogenic SOA precursors (Guenther et al., 2006). Therefore, even though the behavior of S-OOA at different sites might be driven by several parameters, including vegetation coverage, available OA mass, air masses photochemical age and ambient oxidation conditions (e.g. NO_x concentration), temperature seems to be the main driver of S-OOA concentrations. Overall more field observations at other European locations are needed to validate this relation. While the results indicate a probable secondary biogenic origin of the S-OOA factor, the precursors of the B-OOA factor are not identified. In section 4.4.2 more insights into the OOA sources will be discussed.

The S-OOA profile showed a $CO_2^+/C_2H_3O^+$ ratio of 0.61_{avg}, placing it in the region of semi-volatile SOA from biogenic emissions in the *f*44/*f*43 space (Ng et al., 2011), as attributed by Canonaco et al. (2015). Despite the higher summer photochemical activity, the water-soluble bulk OA showed more oxidized mass spectral fingerprints during winter (O:C=0.61_{avg}) than in summer (O:C=0.55_{avg}), similar to the results presented by Canonaco et al. (2015) for Zurich. Accordingly, the S-OOA profile also showed a less oxidized water-soluble mass spectral fingerprint than B-OOA, with an O:C ratio of 0.40_{avg}, in comparison with 0.80_{avg} for B-OOA. Considering the sum of B-OOA and S-OOA, the median OOA:NH_4^+ ratios for Rūgšteliškis, Preila, and Vilnius were 3.2, 2.4, and 2.5 respectively, higher than the average but within the range of the values reported by Crippa et al. (2014) for 25 different European rural sites (2.0_{avg}; minimum value 0.3; maximum 7.3).

4.3 PM_1 source apportionment (marker-PMF)

The PMF factors in this analysis were associated with specific aerosol sources/processes according to their profiles, seasonal trends and relative contributions to the key variables. Fig. 4 displays factor profiles, and the relative contribution of each factor to each variable. The Na^+-rich factor explained a large part of the variability of Ca^{2+}, Mg^{2+}, and Na^+ (Fig. 4) and showed higher contributions during winter than in summer (Fig. 5), suggesting a possible resuspension of sand and salt typically used during winter in Lithuania for road de-icing. This seasonal trend is also consistent with wind speed, which showed the highest monthly values during December 2013 and January 2014. We cannot exclude the possibility that this factor

may include contributions from sea salt, although Na^+ and Cl^- were not enhanced at the marine station in comparison with the other stations. The overall contribution of this Na^+-rich factor to measured PM_1 was relatively small ($1\%_{avg}$), but may be larger in the coarse fraction.

The BB factor showed a well-defined seasonality, with high contributions during winter. This factor explained a large part of the variability of typical wood combustion tracers such as methoxyphenols, sugar anhydrides (including levoglucosan, mannosan, and galactosan), K^+, Cl^-, EC, PAHs, and methyl-PAHs (Fig. 4). Using the $OM{:}OC_{BBOA}$ ratio (1.88) calculated from offline-AMS, we estimated the levoglucosan:BBOC ratio to be 0.18_{avg}, which is within the range of previous studies (Ulevicius et al., 2016 and references therein). Note that this factor explained also large fractions of variables typically associated with non-vehicular fossil fuel combustion, such as benzo(b)naphtho(2,1-d)thiophene (BNT[2,1]) and 6,10,14-trimethyl-2-pentadecanone (DMPT, Fig. 4, Manish et al., 2007; Subramanian et al., 2007), indicating a potential mixing of BB with fossil fuel combustion sources. However, the fossil fuel combustion contribution to BB is unlikely to be large, considering the low concentrations of fossil fuel tracers such as hopanes (66% of the samples below quantification limit (<QL)), BNT[2,1] (64%<QL), and DMPT (55%<QL). Moreover, the above mentioned agreement of the levoglucosan:BBOC ratio with previous studies corroborates the BB estimate from the marker-PMF.

The traffic exhaust factor explained a significant fraction of the alkane variability, with a preferential contribution from light alkanes (Fig. 4). Its contribution was never statistically significant within 3σ. However on average the concentration was higher in Vilnius than at the other stations and in general higher in winter than in summer.

The PBOA factor explained the variability of the primary biological components, such as glucose, mannitol, sorbitol, arabitol, and alkanes with an odd number of carbon atoms (consistent with Bozzetti et al., 2016 and references therein). Highest PBOA concentrations were observed during spring, especially at the rural site of Rūgšteliškis. Overall the contribution of this factor was uncertain with an average relative model error of 160% probably due to the small PBOA contributions ($0.6\%_{avg}$ of the total OM), which hampers a more precise determination by the model. In particular OM_{res} was the variable showing the highest mass contribution to the PBOA factor. However, the large contribution and the large uncertainty of OM_{res} to this factor (0.3 ± 0.4) resulted in a large uncertainty in the PBOA estimated concentration.

The last three factors were related to SA, as indicated by the large contributions of secondary species such as oxalate, SO_4^{2-}, MSA, and NO_3^- to the factor profiles (Fig. 4). The three factors showed different spatial and temporal contributions.

The NO_3^--related SA exhibited highest contributions during winter, suggesting temperature-driven partitioning of secondary aerosol components. Moreover the NO_3^--related SA, similarly to BB and TE, showed the highest concentrations in Vilnius, and the lowest in Rūgšteliškis suggesting its possible relation with anthropogenic gaseous precursors (e.g. NO_x), as already reported in other studies (e.g. Xu et al., 2016; McMeeking et al., 2012).

The MSA-related SA factor manifested the highest concentrations at the marine site of Preila during summer, and in general larger contributions during summer than winter, suggesting its relation with marine secondary aerosol. MSA has been reported to be related to marine secondary biogenic emissions deriving from the photo-oxidation of dimethyl sulfide (DMS) emitted by the phytoplankton bloom occurring during the warm season (Li et al., 1993, Crippa et al., 2013 and references therein).

The last factor (SO_4^{2-}-related SA) showed higher contributions during summer than in winter without clear site-to-site variability, following the seasonal behavior of SO_4^{2-} showing slightly higher concentrations during summer than in winter, which is probably driven by the secondary formation from gaseous photochemical reactions and aqueous phase oxidation. This factor explained the largest part of the oxalate and SO_4^{2-} variability and represented $48\%_{avg}$ of the measured PM_1 by mass.

4.4 Comparison of the source apportionment methods

In this section we compare the offline-AMS PMF and marker-PMF results. We begin with BBOA and TEOA emissions which were resolved by marker-PMF and offline-AMS (TEOA was not resolved by offline-AMS but determined through a CMB approach). The remaining OM fraction (Other-OA = OA – BBOA - TEOA) was apportioned by the offline-AMS source apportionment to B-OOA, S-OOA and LOA ($Other\text{-}OA_{offline\text{-}AMS}$). However, the LOA contribution was statistically significant (within 3σ) only in Vilnius during summer (Table S2), while no data were available for these periods from the marker source apportionment. The marker source apportionment instead attributed the Other-OA mass fraction to 4 factors ($Other\text{-}OA_{marker}$): PBOA, as well as to SO_4^{2-}, NO_3^-, and MSA-related secondary organic aerosols (SOA, Fig. S13). The OA concentrations of the factors retrieved from the PM_1

markers source apportionment were obtained by multiplying the factor time series by the sum of the organic markers and OM_{res} contributions to the normalized factor profiles. The PM concentrations from the marker PMF factors are displayed in Fig. 5.

4.4.1 Primary OA sources

Offline-AMS and marker source apportionments provided comparable BBOA estimates, with concentrations agreeing within a 95% confidence interval (Fig. 6). Results revealed that BBOA contributed the largest fraction to the total OM during winter in Preila and Vilnius, while in Rūgšteliškis the largest OA source derived from B-OOA. The average winter BBOA concentration was 1.1±0.8 μg m^{-3} in Rūgšteliškis and 2±1 μg m^{-3} in Vilnius (errors in this section represent the standard deviation of the temporal variability). Overall the average BBOA concentrations were higher at the urban background site of Vilnius and lower at the rural terrestrial site of Rūgšteliškis. Preila showed higher values (3±3 μg m^{-3}) driven by the grass burning episode occurred at the beginning of March (Ulevicius et al., 2016). Excluding this episode, the BBOA winter concentration was lower than in Vilnius (1.8 μg m^{-3}). During winter, considering only the samples collected concomitantly, Preila and Vilnius showed well correlated BBOA time series (R = 0.91) and significantly positive correlations were observed for also for Preila and Rūgšteliškis (R = 0.72) and for Vilnius and Rūgšteliškis (R = 0.66) (offline-AMS BBOA time series). These results highlight the effect of regional meteorological conditions on the BBOA daily variability in the south east Baltic region.

By contrast, during summer BBOA concentrations were much lower, with 40% of the points showing statistically not significant contributions within 3σ for the offline-AMS source apportionment and 100% for the marker source apportionment. Between late autumn and early March the offline-AMS source apportionment revealed three simultaneous episodes with high BBOA concentrations at the three stations, while the maker source apportionment which is characterized by lower time resolution did not capture some of these episodes. The first episode occurred between 19 and 25 December 2013 during a cold period with an average daily temperature drop to -9.7 °C as measured at the Rūgšteliškis station (no temperature data were available for the other stations). The third episode occurred between 5 and 10 March 2014 and was associated with an intense grass burning episode localized mostly in the Kaliningrad region (Ulevicius et al., 2016, Dudoitis et al., 2016, Mordas et al., 2016).

The episode was not associated with a clear temperature drop, with the highest concentration (14 μg m^{-3}) found at Preila on 10 March 2014, the closest station to the Kaliningrad region. Similarly, at the beginning of February high BBOA concentrations were registered at the three stations, without a clear temperature decrease. Other intense BBOA events were detected but only on a local scale, with intensities comparable to the regional scale episodes. Using the $OM:OC_{BBOA}$ ratio calculated from the HR water-soluble BBOA spectrum (1.88), we estimated the $BBOC_{avg}$ concentrations during the grass burning episode (5-10 March 2014) to span between 0.8 and 7.2 μg m^{-3}. On a daily basis our BBOC concentrations are consistent with the estimated ranges reported by Ulevicius et al. (2016) for non-fossil primary organic carbon (0.6-6.9 μg m^{-3} during the period under consideration), showing also a high correlation (R=0.98).

TEOA estimates obtained by CMB and marker-PMF always agreed with each other within 3σ (Fig. 6). The two approaches confirm that TEOA is a minor source at all three stations (Fig. 6). Hopanes concentrations (used in this work as TEOA tracers) were below detection limits (7 pg m^{-3}) for 66% of the collected samples. Similarly to NO_x, hopanes, showed a clear spatial and seasonal variability with higher concentrations in Vilnius during winter, suggesting an accumulation of traffic emissions in a shallower boundary layer (Fig. 3b, NO_x data available only for Vilnius). During the grass burning event, we observed a peak in the total hopane concentration, and therefore also a peak of the estimated TEOA (2.4 μg m^{-3} maximum value). This relatively high concentration is most probably not due to a local increase of TE, but rather due to a regional transport of polluted air masses from neighboring countries (Poland and the Russian Kaliningrad enclave). By assuming an $OM:OC_{TEOA}$ ratio of 1.2±0.1 (Aiken et al., 2008, Mohr et al., 2008, Docherty et al., 2011, Setyan et al., 2012), we determined the corresponding organic carbon content (TEOC). Our TEOC concentration was consistent within 3σ with the average fossil primary OC over the whole episode estimated by Ulevicius et al. (2016), (0.4-2.1 μg m^{-3}) although on a daily basis the agreement was relatively poor.

Overall, offline-AMS source apportionment and marker-PMF returned comparable results for BBOA and similarly the TEOA estimate by markers-PMF and CMB were comparable, therefore not surprisingly the offline-AMS and marker-PMF approaches yielded OA concentrations also for the Other-OA fractions which agreed within 3σ.

4.4.2 Other-OA sources: offline-AMS and marker-source apportionment comparison

The marker-source apportionment, in comparison to the offline-AMS source apportionment enables resolving well-correlated sources (e.g. BBOA and NO_3^--related SOA) as well as minor sources (e.g. MSA-related SOA and PBOA) because source-specific markers were used as model inputs. By contrast, the offline-AMS source apportionment is capable of resolving OA sources for which no specific markers were available such as LOA, which was separated due to the distinct spatial and temporal trends of some N-containing AMS fragments. We first briefly summarize the Other-OA factor concentrations and their site-to-site differences retrieved by the two techniques; subsequently we compare the two source apportionment results.

The Other-$OA_{offline\text{-}AMS}$ factor time series are displayed in Fig. S13. The B-OOA factor showed relatively stable concentrations throughout the year with $0.9\pm0.8_{avg}$ μg m^{-3} during summer and $1.1\pm0.9_{avg}$ μg m^{-3} during winter. Although B-OOA concentrations were relatively stable throughout the year, higher contributions were observed in Preila and Rūgšteliškis compared to Vilnius. The extreme average seasonal concentrations were between 0.8 and 1.3 μg m^{-3} at Rūgšteliškis during fall and winter, between 0.9 and 1.1 μg m^{-3} at Preila during spring and winter, and between 0.4 and 0.6 μg m^{-3} in Vilnius during summer and winter. These values do not evidence clear seasonal trends, but highlight a site-to-site variability which will be further discussed in the following. S-OOA instead was the largest contributor to total OM during summer with an average concentration of 1.2 ± 0.8 μg m^{-3}, always agreeing between sites within a confidence interval of 95% (2 tails t-test). By contrast, during winter the S-OOA concentration dropped to an average value of 0.3 ± 0.2 μg m^{-3}, with 81% of the points not statistically different from 0 μg m^{-3} within 3σ. Finally, the LOA factor showed statistically significant contributions within 3σ only during summer and late spring in Vilnius. Despite its considerable day-to-day variability this factor contributed 1.0 ± 0.8 μg $m^{-3}{}_{avg}$ in Vilnius during summer.

The markers source apportionment instead attributed $85\%_{avg}$ of the Other-OA_{marker} mass to the SO_4^{2-}-related SOA, while NO_3^--related SOA, MSA-related SOA, and PBOA explained respectively $9\%_{avg}$, $5\%_{avg}$ and $1\%_{avg}$ of the Other-OA_{marker} mass (Fig. S13). The SO_4^{2-}-related SOA average concentration was 2.4 μg m^{-3} during summer and 1.7 μg m^{-3} during winter with

no significant differences from station to station, suggesting a regional origin of the factor. The NO_3^--related SOA concentration was 0.4 μg m^{-3}_{avg} during winter, only 0.03_{avg} μg m^{-3}, during summer, corresponding to $10\%_{avg}$ and 1% of the OA, respectively. Moreover, the NO_3^--related SOA during winter showed the highest average concentrations in Vilnius with 0.5 μg m^{-3} and the lowest in Rūgšteliškis with 0.3 μg m^{-3}_{avg}. The MSA-related SOA instead manifested the highest concentrations during summer with an average of 0.12 μg m^{-3}_{avg}. Higher values were observed during summer at the rural coastal site of Preila where the average concentration was 0.28 μg m^{-3}_{avg} corresponding to $10\%_{avg}$ of the OM. Finally, the PBOA factor exhibited the largest seasonal concentrations during spring at the rural terrestrial site of Rūgšteliškis with an average of 0.05 μg m^{-3}_{avg}, while the summer average concentration was 0.02 μg m^{-3} consistent with the low PBOA estimates reported in Bozzetti et al. (2016) for the submicron fraction during summer.

Many previous studies reported a source apportionment of organic and inorganic markers concentrations (Viana et al., 2008 and references therein). In these studies SO_4^{2-}, NO_3^-, and NH_4^+ were typically used as tracers for secondary aerosol factors commonly associated with regional background and long-range transport; here we compare the apportionment of the SOA factors obtained from the marker source apportionment and the OOA factors separated by the offline-AMS source apportionment. Moreover, contrasting the two source apportionments may provide insight into the origin of the OOA factors retrieved from the offline-AMS source apportionment, and into the origin of the SOA factors resolved by the offline-AMS source apportionment. To our knowledge an explicit comparison has not yet been reported in the literature.

Table 2: Pearson correlation coefficients between Other-OA components from offline-AMS and marker-source apportionment.

		Other-OA_{marker}			
		SO_4^{2-}-related SOA	MSA-related SOA	NO_3^--related SOA	PBOA
Other-$OA_{offline-AMS}$	LOA	0.33	0.16	-0.08	0.10
	B-OOA	0.70	0.22	0.21	0.47
	S-OOA	0.60	0.45	-0.47	0.05

Table 2 reports the correlations between the time series of the Other-OA_{marker} factors and the Other-$OA_{offline-AMS}$ factors (Figs. 6 and S13). These correlations are mostly driven by seasonal

trends as none of these sources shows clear spikes except for LOA during summer in Vilnius. Using the correlations coefficients we can identify the mostly related factors from the two source apportionments.

The SO_4^{2-}-related SOA explained the largest fraction of the Other-OA_{marker} mass ($85\%_{avg}$), and it was the only Other-OA_{marker} factor always exceeding the individual concentrations of B-OOA and S-OOA, indicating that the variability explained by the SO_4^{2-}-related SOA in the marker-source apportionment is explained by both OOA factors in the offline-AMS source apportionment. Moreover, the SO_4^{2-}-related SOA seasonality seems consistent with the sum of S-OOA and B-OOA with higher concentrations in summer than in winter. This observation suggests that the OOA factors resolved by offline-AMS are mostly of secondary origin and the SO_4^{2-}-related SOA, typically resolved by the markersource apportionment, explains the largest fraction of the OOA factors apportioned by offline-AMS which includes both biogenic SOA and aged background OA.

The NO_3^--related SOA and the PBOA were mostly related to the B-OOA factor as they showed higher correlations with B-OOA than with S-OOA. The B-OOA factor therefore may explain a small fraction of primary sources (PBOA), which however represents only $0.6\%_{avg}$ of the total OA. The NO_3^--related SOA and the PBOA were mostly related to the B-OOA factor as they showed higher correlations with B-OOA than with S-OOA. The B-OOA factor therefore may explain a small fraction of primary sources (PBOA), which however represents only $0.6\%_{avg}$ of the total OA. In detail, the NO_3-related SOA correlation with B-OOA was poor (R = 0.21), however the correlation with LOA and S-OOA was negative (Table 2), suggesting that the mass attributed to NO_3-related SOA by the markers source apportionment was fully attributed to the B-OOA factor in the offline-AMS source apportionment. This is also confirmed by the fact that the sum of LOA and S-OOA concentrations during winter (when the NO_3-related SOA substantially contributes) can't explain the NO_3^--related SOA mass, which therefore has to be attributed to B-OOA.

The MSA-related SOA showed the highest correlation with the S-OOA factor, as the two sources exhibited the highest concentrations during summer, although the MSA-related SOA preferentially contributed at the rural coastal site of Preila. While we already discussed the probable secondary biogenic origin of S-OOA, the correlation with the MSA-related SOA suggests that the S-OOA factor, especially at the rural coastal site of Preila, explains also a large fraction of the marine biogenic SOA. The correlation between the two factors is

therefore not surprising as the precursor emissions (dimethyl sulfide, isoprene and terpenes) are strongly related to the temperature leading to higher summer MSA-related SOA and S-OOA concentrations. Assuming all the MSA-related SOA to be explained by the S-OOA factor, we estimate a marine biogenic SOA contribution to S-OOA of $27\%_{avg}$ during summer at Preila, while this contribution is lower at the other stations ($12\%_{avg}$ in Rūgšteliškis during summer, 7% in Vilnius during spring, no summer data for Vilnius Fig. S13). As already mentioned, here we assume all the MSA-related SOA to be related to marine secondary biogenic emissions, however other studies also report MSA from terrestrial biogenic emissions (Jardine et al., 2015), moreover a certain fraction of the MSA-related SOA can also be explained by the B-OOA factor. Overall these findings indicate that the terrestrial sources dominate the S-OOA composition, nevertheless the marine SOA sources may represent a non-negligible fraction, especially at the marine site.

Another advantage obtained in coupling the two source apportionment results is the possibility to study the robustness of the factor analyses by evaluating the consistency of the two approaches as we already discussed for the primary OA and Other-OA fractions. Figure S14a displays the PMF modelled WSOC:measured WSOC PMF for the offline-AMS case, indicating a clear bias between Vilnius and the rural sites, with a WSOC overestimation of ~5% in Preila and Rūgšteliškis. While this overestimation is negligible for WSOC mass, it might have significant consequences on single factor concentrations. By contrast, OM residuals are more homogeneous for the case of markers PMF (Fig. S14b). As we show in Fig. S6, these residuals marginally affect the apportionment of combustion sources, as suggested by the well comparing estimates of BBOA and TEOA using the two methods. Therefore, these residuals are more likely affecting non-combustion sources (LOA, S-OOA and B-OOA). For the common days, the S-OOA concentration is not statistically different at the different stations during summer (confidence interval of 95%), indicating that the residuals are more likely affecting LOA and B-OOA, which instead show site-to-site differences. Now, the PMF WSOC residuals appear at all seasons, also during periods without significant LOA contribution in Vilnius. Therefore, we conclude that B-OOA is the factor most significantly affected by the difference in the WSOC residuals. We could best assess the residual effects by comparing the $\text{B-OOA}_{\text{offline-AMS}}$ with that estimated using the other technique that seem to yield more homogeneous residuals: $\text{B-OOA}_{\text{marker}}$. Here $\text{B-OOA}_{\text{marker}}$ is estimated as $\text{Other-OA}_{\text{markers}}$ - LOA - S-OOA. While $\text{B-OOA}_{\text{offline-AMS}}$ shows site-to-site differences, $\text{B-OOA}_{\text{markers}}$ did not show statistically different concentrations at all stations

within a confidence interval of 95%. Based on these observations, we conclude that observed site-to-site differences in B-OOA concentrations are likely to be related to model uncertainties.

4.5 fCO^+ *vs.* fCO_2^+

Figure 7 displays the water-soluble fCO^+ *vs.* fCO_2^+ scatter plot. A certain correlation (R=0.63) is seen, with fCO_2^+ values being higher than fCO^+ (CO_2^+:CO^+: 1st quartile 1.50, median 1.75, 3rd quartile 2.01), whereas a 1:1 CO_2^+:CO^+ ratio is assumed in standard AMS/ACSM analyses (Aiken et al., 2008; Canagaratna et al., 2007). Comparing the measured CO_2^+:CO^+ values for the bulk WSOM and for pure gaseous CO_2 might provide insight into the origin of the CO^+ fragment in the AMS. The fragmentation of pure gaseous CO_2 returned a CO_2^+:CO^+ ratio of 8.21_{avg} which is significantly higher than our findings for the water-soluble bulk OA (1.75_{med}). Assuming thermal decarboxylation of organic acids as the only source of CO_2^+ does not explain the observed CO_2^+:CO^+ ratio of 1.75_{med} and another large source of CO^+ has to be assumed. Therefore, the carboxylic acid decarboxylation into CO_2 can be considered as a minor source of CO^+.

Figure 7c and Fig. 8 show that not only does the water-soluble (WS) CO_2^+:CO^+ ratio systematically differ from 1, but it also varies throughout the year with higher CO_2^+:CO^+ values associated with warmer temperatures (Fig. 7c). The lower CO_2^+:CO^+ ratios in winter are primarily due to BB, as the WSBBOA factor profile showed the lowest CO_2^+:CO^+ ratio (1.20_{avg}) among all the apportioned WS factors (2.00_{avg} for B-OOA, 2.70_{avg} for S-OOA, and 2.70_{avg} for LOA). We observed a seasonal variation of the CO_2^+:CO^+ ratio also for the water-soluble OOA (S-OOA + B-OOA) mass spectral fingerprint. The CO_2^+:CO^+ ratio was slightly lower for B-OOA than for S-OOA (2.00_{avg} for B-OOA, 2.70 for S-OOA). Nevertheless, given the low S-OOA relative contribution during winter (Fig. 3), we note that the total OOA showed a slightly lower CO_2^+:CO^+ ratio during winter than in summer (Fig. S15), indicating that the OOA mass spectral fingerprint evolves over the year, possibly because of different precursor concentrations, and different photochemical activity.

Fig. 7a shows that most of the measured {fCO^+;fCO_2^+} combinations lies within the triangle defined by the BBOA, S-OOA and B-OOA {fCO^+;fCO_2^+} combinations. The LOA factor {fCO^+;fCO_2^+} combination lies within the triangle as well, but is anyways a minor source and

thus unlikely to contribute to the CO_2^+/CO^+ variability. We parameterized the CO^+ variability as a function of the CO_2^+, and $C_2H_4O_2^+$ fragment variabilities using a multi-parameter fit according to Eq. (8). CO_2^+ and $C_2H_4O_2^+$ were chosen as B-OOA and BBOA tracers, respectively, with B-OOA and BBOA being the factors that explained the largest fraction of the fCO^+ variability (85% together).

$$CO^+_i = a \cdot CO_2^+_i + b \cdot C_2H_4O_2^+_i \quad (8)$$

Although this parameterization is derived from the WSOM fraction CO_2^+, $C_2H_4O_2^+$, and CO^+ originate from the fragmentation of oxygenated, i.e. mostly water-soluble compounds. Accordingly, this parameterization might also well represent the total bulk OA (as the offline-AMS recoveries of these oxygenated fragments are relatively similar: $R_{CO_2^+}$=0.74, $R_{C_2H_4O_2^+}$=0.61, Daellenbach et al., 2016). Note that this parameterization may represent very well the variation of CO^+ in an environment impacted by BBOA and OOA, but should be used with caution when other sources (such as COA) may contribute to CO^+, CO_2^+ and $C_2H_4O_2^+$. In order to check the applicability of this parameterization to a PMF output, we recommend monitoring the CO_2^+ and $C_2H_4O_2^+$ variability explained by the OOA and BBOA factors. In case a large part of the CO_2^+ and $C_2H_4O_2^+$ variability is explained by OOA and BBOA, the parameterization should return accurate CO^+ values. The coefficients *a* and *b* of Eq. (8) were determined as 0.52 and 1.39 respectively, while the average fit residuals were estimated to be equal to 10% (Fig. S16). In contrast, parameterizing CO^+ as proportional to CO_2^+ only (as done in the standard AMS analysis scheme with coefficients updated to the linear fit between CO^+ and CO_2^+ (1.75)) yielded $20\%_{avg}$ residuals, indicating that such a univariate function describes the CO^+ variation less precisely.

An alternative parameterization is presented in the SI in which the contribution of moderately oxygenated species (such as S-OOA) to CO^+ was also considered by using $C_2H_3O^+$ as an independent variable. We show that the dependence of CO^+ on $C_2H_3O^+$ is statistically significant (Fig. 7c) as also suggested by the PMF results (S-OOA contributes 12% to the CO^+ variability). However, the parameter relating CO^+ to $C_2H_3O^+$ is negative, because the CO^+:CO_2^+ and CO^+:$C_2H_4O_2^+$ ratios are lower in moderately oxygenated species compared to species present in BBOA and B-OOA. While this parameterization captures the variability of CO^+ across the seasons better compared to a 2-parameter fit for the present dataset, it may be more prone to biases in other environments due to the known contributions of other factors to $C_2H_3O^+$. For example, cooking-influenced organic aerosol (COA) often accounts for a

significant fraction of $C_2H_3O^+$. For ambient datasets we propose the use of CO_2^+ and $C_2H_4O_2^+$ only, which may capture less variation but is also less prone to biases. Although our results suggest that the available CO^+ and O:C estimates (Aiken et al., 2008; Canagaratna et al., 2015) may not well capture the CO^+ variability, our CO^+ parameterization should not be applied to calculate the O:C ratios or recalculate the OA mass from AMS datasets, as those are calibrated assuming a standard fragmentation table (i.e. $CO_2^+ = CO^+$).

In a recent work, Canagaratna et al. (2015) reported the Ar nebulization of water soluble single compounds to study the HR-AMS mass spectral fingerprints in order to improve the calculation of O:C and OM:OC ratios. Following the same procedure, we nebulized a subset of the same standard compounds including malic acid, azalaic acid, citric acid, tartaric acid, cis-pinonic acid, and D(+)-mannose. We obtained comparable CO_2^+:CO^+ ratios (within 10%) to those of Canagaratna et al. (2015) for all the analyzed compounds, highlighting the comparability of results across different instruments. With the exception of some multifunctional compounds (citric acid, malic acid tartaric acid, ketobutyric acid, hydroxyl methylglutaric acid, pyruvic acid, oxaloacetic acid, tartaric acid, oxalic acid and malonic acid), the water-soluble single compounds analyzed by Canagaratna et al. (2015) mostly showed CO_2^+:CO^+ ratios <1, systematically lower than the CO_2^+:CO^+ ratios measured for the bulk WSOM in Lithuania (1st quartile 1.50, median 1.75, 3rd quartile 2.01), which represents a large fraction of the total OM (bulk EE: median = 0.59, 1st quartile = 0.51, 3rd quartile = 0.72). Considering the relatively high extraction efficiency, and considering that the CO^+ and CO_2^+ fragmentation precursors tend to be more water soluble than the bulk OA, the aforementioned compounds could be representative of a large part of the CO^+ and CO_2^+ fragmentation precursors. This indicates that the selection of appropriate reference compounds for ambient OA is non-trivial, and the investigation of multifunctional compounds is of high importance.

5 Conclusions

PM_1 filter samples were collected over an entire year (November 2013 to October 2014) at three different stations in Lithuania. Filters were analyzed by water extraction followed by nebulization of the liquid extracts and subsequent measurement of the generated aerosol with an HR-ToF-AMS (Daellenbach et al., 2016). For the first time, the nebulization step was conducted in Ar, enabling direct measurement of the CO^+ ion, which is typically masked by N_2^+ in ambient air and assumed to be equal to CO_2^+ (Aiken et al., 2008). CO_2^+:CO^+ values >1

were systematically observed, with a mean ratio of 1.7±0.3. This is likely an upper limit for ambient aerosol, as only the water-soluble OM fraction is measured by the offline-AMS technique. CO^+ concentrations were parameterized as a function of CO_2^+, and $C_2H_4O_2^+$, and this two-variable parameterization showed a superior performance to a parameterization based on CO_2^+ alone, because CO^+ and CO_2^+ show different seasonal trends.

PMF analysis was conducted on both the offline-AMS data described above and a set of molecular markers together with total OM. Biomass burning was found to be the largest OM source in winter, while secondary OA was largest in summer. However, higher concentrations of primary anthropogenic sources (biomass burning and hopanes here used as traffic markers) were found at the urban background station of Vilnius. The offline-AMS and marker-based analyses also identified local emissions and primary biological particles, respectively, as factors with low overall but episodically important contributions to PM. Both methods showed traffic exhaust emissions to be only minor contributors to the total OM; which is not surprising given the distance of the three sampling stations from busy roads.

The two PMF analyses apportioned SOA to sources in different ways. The offline-AMS data yielded factors related to regional background (B-OOA) and temperature-driven (likely biogenic-influenced) emissions (S-OOA), while the marker-PMF yielded factors related to nitrate, sulfate, and MSA. For the offline-AMS PMF, S-OOA was the dominant factor in summer and showed a positive exponential correlation with the average daily temperature, similar to the behavior observed by Leaitch et al. (2011) in a Canadian boreal forest. Combining the two source apportionment techniques suggests that the S-OOA factor includes contributions from both terrestrial and marine secondary biogenic sources, while only small PBOA contributions to submicron OOA factors are possible. The analysis highlights the importance of regional meteorological conditions on air pollution in the southeastern Baltic region, as evidenced by simultaneous high BBOA levels at the three stations during three different episodes in winter and by statistically similar S-OOA concentrations across the three stations during summer.

Acknowledgements

The research leading to these results received funding from the Lithuanian–Swiss Cooperation Programme “Research and Development” project AEROLIT (Nr. CH-3-ŠMM-01/08). JGS acknowledges the support of the Swiss National Science Foundation (Starting

Grant No. BSSGI0 155846). IE-H acknowledges the support of the Swiss National Science Foundation (IZERZ0 142146).

References

Aiken, A. C., DeCarlo, P. F., Kroll, J. H., Worsnop, D. R., Huffmann, J. A., Docherty, K. S., Ulbrich, I. M., Mohr, C., Kimmel, J. R., Sueper, D., Sun, Y., Zhang, Q., Trimborn, A., Northway, M., Ziemann, P. J., Canagaratna, M. R., Onasch, T. B., Alfarra, M. R., Prevot, A. S. H., Dommen, J., Duplissy, J., Metzger, A., Baltensperger, U., and Jimenez J. L. O/C and OM:OC ratios of primary, secondary, and ambient organic aerosols with high-resolution time-of-flight aerosol mass spectrometry. Environ. Sci. Technol. 42, 4478-4485, 2008.

Aksoyoglu, S., Keller, J., Barmpadimos, I., Oderbolz, D., Lanz, V. A., Prévôt, A. S. H., and Baltensperger U.: Aerosol modelling in Europe with a focus on Switzerland during summer and winter episodes, Atmos. Chem. Phys., 11, 7355–7373, 2011.

Aksoyoglu, S., Keller, J., Ciarelli, G., Prévôt, A. S. H., and Baltensperger, U.: A model study on changes of European and Swiss particulate matter, ozone and nitrogen deposition between 1990 and 2020 due to the revised Gothenburg protocol, Atmos. Chem. Phys., 14, 13081-13095, doi:10.5194/acp-14-13081-2014, 2014.

Alfarra, M. R., Prévôt, A. S. H., Szidat, S., Sandradewi, J., Weimer, S., Lanz, V. A., Schreiber, D., Mohr, M., and Baltensperger, U.: Identification of the mass spectral signature of organic aerosols from wood burning emissions, Environ. Sci. Technol., 41, 5770–5777, 2007.

Allan, J. D., Delia, A. E., Coe, H., Bower, K. N., Alfarra, M. R., Jimenez, J. L., Middlebrook, A. M., Drewnick, F., Onasch, T. B., and Canagaratna, M. R.: A generalized method for the extraction of chemically resolved mass spectra from Aerodyne aerosol mass spectrometer data, J. Aerosol Sci. 35 , 909-922, 2004.

Allan, J. D., Jimenez, J. L., Williams, P. I., Alfarra, M. R., Bower, K. N., Jayne, J. T., Coe, H., and Worsnop, D. R.: Quantitative sampling using an Aerodyne aerosol mass spectrometer: 1. Techniques of data interpretation and error analysis, J. Geophys. Res.-Atmos., 108, 4090, 2003.

Baklanov, A., Schlünzen, K., Suppan, P., Baldasano, J., Brunner, D., Aksoyoglu, S., Carmichael, G., Douros, J., Flemming, J., Forkel, R., Galmarini, S., Gauss, M., Grell, G., Hirtl, M., Joffre, S., Jorba, O., Kaas, E., Kaasik, M., Kallos, G., Kong, X., Korsholm, U., Kurganskiy, A., Kushta, J., Lohmann, U., Mahura, A., Manders-Groot, A., Maurizi, A., Moussiopoulos, N., Rao, S. T., Savage, N., Seigneur, C., Sokhi, R. S., Solazzo, E.,

Solomos, S., Sørensen, B., Tsegas, G., Vignati, E., Vogel, B., and Zhang, Y.: Online coupled regional meteorology chemistry models in Europe: current status and prospects, Atmos. Chem. Phys., 14, 317-398, doi:10.5194/acp-14-317-2014, 2014.

Besombes, J.-L., Maître, A., Patissier, O., Marchand, N., Chevron, N., Stoklov, M., Masclet, P.: Particulate PAHs observed in the surrounding of a municipal incinerator. Atmos. Environ. 35, 6093–6104, 2001.

Birch, M. E. and Cary, R. A.: Elemental carbon-based method for monitoring occupational exposures to particulate diesel exhaust, Aerosol Sci. and Tech., 25, 221–241, 1996.

Bozzetti, C., Daellenbach, K., R., Hueglin, C., Fermo, P., Sciare, J., Kasper-Giebl, A., Mazar, Y., Abbaszade, G., El Kazzi, M., Gonzalez, R., Shuster Meiseles, T., Flasch, M., Wolf, R., Křepelová, A., Canonaco, F., Schnelle-Kreis, J., Slowik, J. G., Zimmermann, R., Rudich, Y., Baltensperger, U., El Haddad, I., and Prévôt, A. S. H.: Size-Resolved Identification, Characterization, and Quantification of Primary Biological Organic Aerosol at a European Rural Site, Environ. Sci. Technol., doi: 10.1021/acs.est.5b05960, 2016.

Bressi, M., Sciare, J., Ghersi, V., Mihalopoulos, N., Petit, J.-E., Nicolas, J. B., Moukhtar, S., Rosso, A., Féron, A., Bonnaire, N., Poulakis, E., and Theodosi, C.: Sources and geographical origins of fine aerosols in Paris (France), Atmos. Chem. Phys., 14, 8813–8839, 2014.

Brown, S. G., Eberly, S., Paatero, P., and Norris, G. A., Methods for estimating uncertainty in PMF solutions: Examples with ambient air and water quality data and guidance on reporting PMF results, Sci. Tot. Environ. 518-519, 626-635, 2015.

Bruns, E. A., Krapf, M., Orasche, J., Huang, Y., Zimmermann, R., Drinovec, L., Močnik, G., El-Haddad, I., Slowik, J. G., Dommen, J., Baltensperger, U. and Prévôt, A. S. H.: Characterization of primary and secondary wood combustion products generated under different burner loads, Atmos. Chem. Phys., 15, 2825–2841, 2015.

Budisulistiorini, S. H., Canagaratna, M. R., Croteau, P. L., Marth, W. J., Baumann, K., Edgerton, E. S., Shaw, S. L., Knipping, E. M., Worsnop, D. R., Jayne, J. T., Gold, A., and Surratt, J. D.: Real-Time Continuous Characterization of Secondary Organic Aerosol Derived from Isoprene Epoxydiols in Downtown Atlanta, Georgia, Using the Aerodyne Aerosol Chemical Speciation Monitor, Environ Sci Technol, 47, 5686-5694, Doi 10.1021/Es400023n, 2013.

Byčenkienė, S., Ulevicius, V., Plauškaitė, K., Bozzetti, C., Fröhlich, R., Mordas, G., Slowik, J. G., El Haddad, I., Canonaco, F., and Prévôt A. S. H.: Source apportionment of the carbonaceous aerosols during wintertime over urban environment, *in prep*.

Canagaratna, M. R., Jayne, J. T., Jimenez, J. L., Allan, J. D., Alfarra, M. R., Zhang, Q., Onasch, T. B., Drewnick, F., Coe, H., Middlebrook, A., Delia, A., Williams, L. R., Trimborn, A. M., Northway, M. J., DeCarlo, P. F., Kolb, C. E., Davidovits, P. and Worsnop, D. R.: Chemical and microphysical characterization of ambient aerosols with the Aerodyne aerosol mass spectrometer, Mass Spectrom. Rev. 26:185-222, 2007.

Canagaratna, M. R., Jimenez, J. L., Kroll, J. H., Chen, Q., Kessler, S. H., Massoli, P., Hildebrandt Ruiz, L., Fortner, E., Williams, L. R., Wilson, K. R., Surratt, J. D., Donahue, N. M., Jayne, J. T., and Worsnop, D. R.: Elemental ratio measurements of organic compounds using aerosol mass spectrometry: characterization, improved calibration, and implications, Atmos. Chem. Phys., 15, 253-272, doi:10.5194/acp-15-253-2015, 2015.

Canonaco, F., Crippa, M., Slowik, J. G., Baltensperger, U., and Prévôt, A. S. H.: SoFi, an IGOR-based interface for the efficient use of the generalized multilinear engine (ME-2) for the source apportionment: ME-2 application to aerosol mass spectrometer data, Atmos. Meas. Tech., 6, 3649-3661, 2013.

Canonaco, F., Slowik, J. G., Baltensperger, U., and Prévôt, A. S. H.: Seasonal differences in oxygenated organic aerosol composition: implications for emissions sources and factor analysis. Atmos. Chem. Phys. 15, 6993-7002, 2015.

Cavalli, F., Viana, M., Yttri, K. E., Genberg, J., and Putaud, J. P.: Toward a standardised thermal-optical protocol for measuring atmospheric organic and elemental carbon: the EUSAAR protocol, Atmos. Meas. Tech., 3, 79-89, 2010.

Chow, J., Watson, J., Ashbaugh, L. L., and Magliano, K. L.: Similarities and differences in PM10 chemical source profiles for geological dust from the San Joaquin Valley, California. Atmos. Environ. 37, 1317-1340, 2003.

Crippa, M., Canonaco, F., Lanz, V. A., Äijälä, M., Allan, J. D., Carbone, S., Capes, G., Ceburnis, D., Dall'Osto, M., Day, D. A., DeCarlo, P. F., Ehn, M., Eriksson, A., Freney, E., Hildebrandt Ruiz, L., Hillamo, R., Jimenez, J. L., Junninen, H., Kiendler-Scharr, A., Kortelainen, A. M., Kulmala, M., Laaksonen, A., Mensah, A. A., Mohr, C., Nemitz, E., O'Dowd, C., Ovadnevaite, J., Pandis, S. N., Petäjä, T., Poulain, L., Saarikoski, S., Sellegri, K.,

Swietlicki, E., Tiitta, P., Worsnop, D. R., Baltensperger, U., and Prévôt, A. S. H.: Organic aerosol components derived from 25 AMS data sets across Europe using a consistent ME-2 based source apportionment approach, Atmos. Chem. Phys., 14, 6159–6176, 2014.

Crippa, M., El Haddad, I., Slowik, J. G., DeCarlo, P.F., Mohr, C., Heringa, M. F., Chirico, R., Marchand, N., L., Sciare, J., Baltensperger, U., and Prévôt, A. S. H.: Identification of marine and continental aerosol sources in Paris using high resolution aerosol mass spectrometry, J. Geophys. Res., 118, 1950-1963, 2013.

Daellenbach, K. R., Bozzetti, C., Krepelova, A., Canonaco, F., Huang, R.-J., Wolf, R., Zotter, P., Crippa, M., Slowik, J., Zhang, Y., Szidat, S., Baltensperger, U., Prévôt, A. S. H., and El Haddad, I.: Characterization and source apportionment of organic aerosol using offline aerosol mass spectrometry, Atmos. Meas. Tech., 9, 23-39, 2016.

Davison, A. C. and Hinkley, D. V.: Bootstrap Methods and Their Application, Cambridge University Press, Cambridge, UK, 582 pp., 1997.

DeCarlo, P. F., Kimmel, J. R., Trimborn, A., Northway, M. J., Jayne, J. T., Aiken, A. C., Gonin, M., Fuhrer, K., Horvath, T., Docherty, K. S., Worsnop, D. R., and Jimenez, J. L.: Field-deployable, high-resolution, time-of-flight aerosol mass spectrometer, Anal. Chem., 78, 8281–8289, 2006.

Dockery, D. W., Luttmann-Gibson, H., Rich, D. Q., Link, M. S., Mittleman, M. A., Gold, D. R., Koutrakis, P., Schwartz, J. D., and Verrier, R. L.: Association of air pollution with increased incidence of ventricular tachyarrhythmias recorded by implanted cardioverter defibrillators, Environ. Health Perspect. 113:670-674, 2005.

Docherty, K. S., Aiken, A. C., Huffman, J. A., Ulbrich, I. M., DeCarlo, P. F., Sueper, D., Worsnop, D. R., Snyder, D. C., Peltier, R. E., Weber, R. J., Grover, B. D., Eatough, D. J., Williams, B. J., Goldstein, A. H., Ziemann, P. J., and Jimenez, J. L.: The 2005 Study of Organic Aerosols at Riverside (SOAR-1): instrumental intercomparisons and fine particle composition, Atmos. Chem. Phys., 11, 12387-12420, doi:10.5194/acp-11-12387-2011, 2011.

Dudoitis, V., Byčenkienė, S., Plauškaitė, K., Bozzetti, C., Fröhlich, R., Mordas, G., and Ulevicius V.: Spatial distribution of carbonaceous aerosol in the southeastern Baltic region (event of grass fires), Acta Geophys., 64, 711-731, 2016.

El Haddad, I., D'Anna, B., Temime-Roussel, B., Nicolas, M., Boreave, A., Favez, O., Voisin, D., Sciare, J., George, C., Jaffrezo, J.-L., Wortham, H., and Marchand, N.: Towards a better

1 understanding of the origins, chemical composition and aging of oxygenated organic aerosols:
2 case study of a Mediterranean industrialized environment, Marseille, Atmos. Chem. Phys., 13,
3 7875-7894, doi:10.5194/acp-13-7875-2013, 2013.

4 El Haddad, I., Marchand, N., Dron, J., Temime-Roussel, B., Quivet, E., Wortham, H.,
5 Jaffrezo, J. L., Baduel, C., Voisin, D., Besombes, J. L., and Gille, G.: Comprehensive primary
6 particulate organic characterization of vehicular exhaust emissions in France, Atmos.
7 Environ., 43, 6190–6198, 2009.

8 Elser, M., Bozzetti, C., El-Haddad, I., Maasikmets, M., Teinemaa, E., Richter, R., Wolf, R.,
9 Slowik, J. G., Baltensperger, U., and Prévôt, A. S. H.: Urban increments of gaseous and
10 aerosol pollutants and their sources using mobile aerosol mass spectrometry measurements,
11 Atmos. Chem. Phys. Discuss., doi:10.5194/acp-2016-31, 2016.

12 Elser, M., Huang, R.-J., Wolf, R., Slowik, J. G., Wang, Q., Canonaco, F., Li, G., Bozzetti, C.,
13 Daellenbach, K. R., Huang, Y., Zhang, R., Li, Z., Cao, J., Baltensperger, U., El-Haddad, I.,
14 and Prévôt, A. S. H.: New insights into PM2.5 chemical composition and sources in two
15 major cities in China during extreme haze events using aerosol mass spectrometry, Atmos.
16 Chem. Phys., 16, 3207-3225, doi:10.5194/acp-16-3207-2016, 2016.

17 Fraser, M. P., Cass, G. R., and Simoneit, B. R. T.: Gas-phase and particle-phase organic
18 compounds emitted from motor vehicle traffic in a Los Angeles roadway tunnel, Environ. Sci.
19 Technol. 14, 2051-2060, 1998.

20 Fröhlich, R., Cubison, M. J., Slowik, J. G., Bukowiecki, N., Prevot, A. S. H., Baltensperger,
21 U., Schneider, J., Kimmel, J. R., Gonin, M., Rohner, U., Worsnop, D. R. and Jayne J. T.: The
22 ToF-ACSM: a portable aerosol chemical speciation monitor with TOFMS detection, Atmos.
23 Meas. Tech., 6, 3225-3241, 2013.

24 Golly, B., Brulfert, G., Berlioux G., Jaffrezo J.-L., Besombes, J.-L.: Large chemical
25 characterisation of PM10 emitted from graphite material production: Application in source
26 apportionment, Sci. Tot. Environ., 538, 634–643, 2015.

27 Guenther, A., Karl, T., Harley, P., Wiedinmyer, C., Palmer, P. I., and Geron, C.: Estimates of
28 global terrestrial isoprene emissions using MEGAN (Model of Emissions of Gases and
29 Aerosols from Nature), Atmos. Chem. Phys., 6, 3181-3210, doi:10.5194/acp-6-3181-2006,
30 2006.

He, L.-Y., Hu, M., Zhang, Y.-H., Huang, X.-F. and Yao, T.-T: Chemical characterization of fine particles from on-road vehicles in the Wutong tunnel in Shenzhen, China, Chemosphere 62, 1565-1573, 2006.

He, L.-Y., Hu, M., Zhang, Y.-H., Huang, X.-F., and Yao, T.-T. Fine particle emissions from onroad vehicles in the Zhujiang tunnel, China, Environ. Sci. Technol., 42, 4461-4466, 2008.

Herich, H., Gianini, M. F. D., Piot, C., Močnik, G., Jaffrezo, J. L., Besombes, J. L., Prévôt, A. S. H., and Hueglin, C.: Overview of the impact of wood burning emissions on carbonaceous aerosols and PM in large parts of the Alpine region, Atmos. Environ., 89, 64–75, doi:10.1016/j.atmosenv.2014.02.008, 2014.

Hu, W. W., Campuzano-Jost, P., Palm, B. B., Day, D. A., Ortega, A. M., Hayes, P. L., Krechmer, J. E., Chen, Q., Kuwata, M., Liu, Y. J., de Sá, S. S., McKinney, K., Martin, S. T., Hu, M., Budisulistiorini, S. H., Riva, M., Surratt, J. D., St. Clair, J. M., Isaacman-Van Wertz, G., Yee, L. D., Goldstein, A. H., Carbone, S., Brito, J., Artaxo, P., de Gouw, J. A., Koss, A., Wisthaler, A., Mikoviny, T., Karl, T., Kaser, L., Jud, W., Hansel, A., Docherty, K. S., Alexander, M. L., Robinson, N. H., Coe, H., Allan, J. D., Canagaratna, M. R., Paulot, F., and Jimenez, J. L.: Characterization of a real-time tracer for isoprene epoxydiols-derived secondary organic aerosol (IEPOX-SOA) from aerosol mass spectrometer measurements, Atmos. Chem. Phys., 15, 11807-11833, 10.5194/acp-15-11807-2015, 2015.

Huang, R.-J., Zhang, Y., Bozzetti, C., Ho, K.-F., Cao, J., Han, Y., Dällenbach, K. R., Slowik, J. G., Platt, S. M., Canonaco, F., Zotter, P., Wolf, R., Pieber, S. M., Bruns, E. A., Crippa, M., Ciarelli, G., Piazzalunga, A., Schwikowski, M., Abbaszade, G., Schnelle-Kreis, J., Zimmermann, R., An, Z., Szidat, S., Baltensperger, U., Haddad, I. E., and Prévôt, A. S. H.: High secondary aerosol contribution to particulate pollution during haze events in China, Nature, 514, 2014.

Jaffrezo, J.-L., Aymoz, G., Delaval, C., and Cozic J.: Seasonal evolution of the soluble fraction of particulate organic carbon in Alpine Valleys. Atmos. Chem. Phys., 5, 2809-2821, 2005.

Jaffrezo, J. L., Calas, T., and Bouchet, M.: Carboxylic acids measurements with ionic chromatography, Atmos. Environ., 32, 2705–2708, 1998.

Jardine, K., Yañez-Serrano, A. M., Williams, J., Kunert, N., Jardine, A., Taylor, T., Abrell, L., Artaxo, P., Guenther, A., Hewitt, C. N., House, E., Florentino, A. P., Manzi, A., Higuchi,

N., Kesselmeier, J., Behrendt, T, Veres, P. R., Derstroff, B., Fuentes, J. D., Martin, S. T., and Andreae, M. O.: Dimethyl Sulfide in the Amazon Rain Forest, Global Biogeochem. Cy., 29, 19-32, 2015.

Klein, F., Platt, S. M., Farren, N. J., Detournay, A., Bruns, E. A., Bozzetti, C., Daellenbach, K. R., Kilic, D., Kumar, N. K., Pieber, S. M., Slowik, J. G., Temime-Roussel, B., Marchand, N., Hamilton, J. F., Baltensperger, U., Prévôt, A. S. H., and El Haddad, I.: Characterization of gas-phase organics using proton transfer reaction time-of-flight mass spectrometry: cooking emissions, Environ. Sci. Technol., 50, 1243–1250, 2016.

Laden, F., Neas, L. M., Dockery, D. W., and Schwartz, J.: Association of fine particulate matter from different sources with daily mortality in six US cities, Environ. Health Perspect. 108:941-947, 2000.

Lanz, V. A., Alfarra, M. R., Baltensperger, U., Buchmann, B., Hueglin, C., and Prévôt, A. S. H.: Source apportionment of submicron organic aerosols at an urban site by factor analytical modelling of aerosol mass spectra, Atmos. Chem. Phys., 7, 1503-1522, doi:10.5194/acp-7-1503-2007, 2007.

Lanz, V. A., Prévôt, A. S. H., Alfarra, M. R., Weimer, S., Mohr, C., DeCarlo, P. F., Gianini, M. F. D., Hueglin, C., Schneider, J., Favez, O., D'Anna, B., George, C., and Baltensperger, U.: Characterization of aerosol chemical composition with aerosol mass spectrometry in Central Europe: an overview, Atmos. Chem. Phys., 10, 10453–10471, 2010.

Leaitch, W. R. Macdonald, A. M., Brickell, P. C., Liggio, J., Sjostedt, S. J., Vlasenko, A., Bottenheim, J. W., Huang, L., Li, S.-M., Liu, P. S. K., Toom-Sauntry, D., Hayden, K. A., Sharma, S., Shantz, N. C., Wiebe H. A., Zhang, W., Abbatt, J. P. D., Slowik, J. G., Chang, Rachel, Y.-W., Russell, L. M., Schwartz, R. E., Takahama, S., Jayne, J. T., Ng, N. L.: Temperature response of the submicron organic aerosol from temperate forests, Atmos. Environ., 45, 6696-6704, 2011.

Lee, A. K. Y., Herckes, P., Leaitch, W. R., Macdonald, A. M., and Abbatt, J. P. D.: Aqueous OH oxidation of ambient organic aerosol and cloud water organics: Formation of highly oxidized products, Geoph. Res. Lett., 38, L11 805, 2011.

Li, S.M., Talbot, R.W., Barrie, L.A., Harriss, R.C., Davidson, C.I. and Jaffrezo, J.-L.: Seasonal and geographic variations of methanesulfonic acid in the Arctic troposphere, Atmos. Environ., 27A, 3011-3024, 1993.

Lohmann, U., Broekhuizen, K., Leaitch, R., Shantz, N., and Abbatt, J.: How efficient is cloud droplet formation of organic aerosols?, Geophys. Res. Lett. 31, L05108, 2004.

Manish K. S., Subramanian, R., Rogge, W. F., and Robinson, A. L.: Sources of organic aerosol: Positive matrix factorization of molecular marker data and comparison of results from different source apportionment models, Atmos. Environ., 41, 9353-9369, 2007.

McMeeking, G. R., Bart, M., Chazette, P., Haywood, J. M.,, Hopkins, J. R., McQuaid, J. B., Morgan, W. T., Raut, J.-C., Ryder, C. L., Savage, N., Turnbull, K., and Coe, H.: Airborne measurements of trace gases and aerosols over the London metropolitan region, Atmos. Chem. Phys., 12, 5163–5187, 2012.

Mihara, T. and Mochida, M.: Characterization of solvent-extractable organics in urban aerosols based on mass spectrum analysis and hygroscopic growth measurement, Envir. Sci. Tech., 45, 9168–9174, 2011.

Minguillón, M. C., Perron, N., Querol, X., Szidat, S., Fahrni, S. M., Alastuey, A., Jimenez, J. L., Mohr, C., Ortega, A. M., Day, D. A., Lanz, V. A., Wacker, L., Reche, C., Cusack, M., Amato, F., Kiss, G., Hoffer, A., Decesari, S., Moretti, F., Hillamo, R., Teinila, K., Seco, R., Penuelas, J., Metzger, A., Schallhart, S., Muller, M., Hansel, A., Burkhart, J. F., Baltensperger, U., and Prevot, A. S. H.: Fossil versus contemporary sources of fine elemental and organic carbonaceous particulate matter during the DAURE campaign in Northeast Spain, Atmos. Chem. Phys., 11, 12067-12084, 2011.

Mohr, C., DeCarlo, P. F., Heringa, M. F., Chirico, R., Slowik, J. G., Richter, R., Reche, C., Alastuey, A., Querol, X., Seco, R., Penuelas, J., Jimenez, J. L., Crippa, M., Zimmermann, R., Baltensperger, U., and Prevot, A. S. H.: Identification and quantification of organic aerosol from cooking and other sources in Barcelona using aerosol mass spectrometer data, Atmos. Chem. Phys., 12, 1649-1665, 2012.

Mordas, G., Plauškaitė, K., Prokopčiuk, N., Dudoitis, V., Bozzetti, C. and Ulevicius, V.: Observation of new particle formation on Curonian Spit located between continental Europe and Scandinavia, J Aerosol Sci, 97, 38-55, 2016.

Ng, N. L., Herndon, S. C., Trimborn, A., Canagaratna, M. R., Croteau, P. L., Onasch, T. B. Sueper, D., Worsnop, D. R., Zhang, Q., Sun, Y. L. and Jayne, J. T.: An Aerosol Chemical Speciation Monitor (ACSM) for routine monitoring of the composition and mass concentrations of ambient aerosol, Aerosol Sci. Tech., 45, 770-784, 2011.

Paatero, P.: Least squares formulation of robust non-negative factor analysis, Chemom. Intell. Lab. Syst., 37, 23–35, 1997.

Paatero, P.: The multilinear engine - A table-driven, least squares program for solving multilinear problems, including the n-way parallel factor analysis model, J. Comput. Graph. Stat., 8, 854-888, 1999.

Paatero, P. and Tapper, U.: Positive matrix factorization - a nonnegative factor model with optimal utilization of error-estimates of data values, Environmetrics, 5, 111-126, 1994.

Rocke, D. M., and Lorenzato, S.: A two-component model for measurement error in analytical chemistry, Technometrics, 37, 176-184, 1995.

Rutter, A. P., Snyder, D. C., Schauer, J. J., DeMinter, J. and Shelton, B.: Sensitivity and bias of molecular marker-based aerosol source apportionment models to small contributions of coal combustion soot, Environ. Sci. Technol., 43, 7770-7777, 2009.

Schauer, J. J., Kleeman, M. J., Cass, G. R., and Simoneit, B. T.: Measurement of emissions from air pollution sources. 3. C1-C29 organic compounds from fireplace combustion of wood, Environ. Sci. Technol., 35, 1716-1728, 2001.

Schwarze, P. E., Ovrevik, J., Lag, M., Refsnes, M., Nafstad, P., Hetland, R. B., and Dybing, E.: Particulate matter properties and health effects: consistency of epidemiological and toxicological studies, Hum. Exp. Toxicol. 25, 559-579, 2006.

Setyan, A., Zhang, Q., Merkel, M., Knighton, W. B., Sun, Y., Song, C., Shilling, J. E., Onasch, T. B., Herndon, S. C., Worsnop, D. R., Fast, J. D., Zaveri, R. A., Berg, L. K., Wiedensohler, A., Flowers, B. A., Dubey, M. K., and Subramanian R.: Characterization of submicron particles influenced by mixed biogenic and anthropogenic emissions using high-resolution aerosol mass spectrometry: results from CARES, Atmos. Chem. Phys., 12, 8131-8156, 2012.

Subramanian, R., Donahue, N. M., Bernardo-Bricker, A., Rogge, W. F., and Robinson, A. L.: Contribution of motor vehicle emissions to organic carbon and fine particle mass in Pittsburgh, Pennsylvania: Effects of varying source profiles and seasonal trends in ambient marker concentrations, Atmos. Environ., 40, 8002-8019, 2006.

Subramanian, R., Donahue, N. M., Bernardo-Bricker, A., Rogge, W. F., and Robinson, A. L.: Insights into the primary-secondary and regional-local contributions to organic aerosol and $PM_{2.5}$ mass in Pittsburgh, Pennsylvania, Atmos. Environ., 41, 7414-7433, 2007.

Sun, Y., Zhang, Q., Zheng, M., Ding, X., Edgerton, E. S., and Wang, X.: Characterization and source apportionment of water-soluble organic matter in atmospheric fine particles (PM2.5) with High-Resolution Aerosol Mass Spectrometry and GC-MS, Envir. Sci. Tech., 45, 4854–4861, 2011.

Ulbrich, I. M., Canagaratna, M. R., Zhang, Q., Worsnop, D. R., and Jimenez, J. L.: Interpretation of organic components from positive matrix factorization of aerosol mass spectrometric data, Atmos. Chem. Phys., 9, 2891-2918, 2009.

Ulevicius, V., Byčenkienė, S., Bozzetti, C., Vlachou, A., Plauškaitė, K., Mordas, G., Dudoitis, V., Abbaszade, G., Remeikis, V., Garbaras, A., Masalaite, A., Blees, J., Fröhlich, R., Dällenbach, K. R., Canonaco, F., Slowik, J. G., Dommen, J., Zimmermann, R., Schnelle-Kreis, J., Salazar, G. A., Agrios, K., Szidat, S., El Haddad, I., and Prévôt, A. S. H.: Fossil and non-fossil source contributions to atmospheric carbonaceous aerosols during extreme spring grassland fires in Eastern Europe. Atmos. Chem. Phys., 16, 5513-5529, 2016.

Viana, M., Kuhlbusch, T. A. J., Querol, X., Alastuey, A., Harrison, R. M., Hopke, P. K., Winiwarter, W., Vallius, M., Szidat, S., Prévôt, A. S. H., Hueglin, C., Bloemen, H., Wåhlin, P., Vecchi, R., Miranda, A. I., Kasper-Giebl, A., Maenhaut, W., and Hitzenberger, R.: Source apportionment of particulate matter in Europe: a review of methods and results, J. Aerosol Sci., 39, 827–849, doi:10.1016/j.jaerosci.2008.05.007, 2008.

Waked, A., Favez, O., Alleman, L. Y., Piot, C., Petit, J. E., Delaunay, T., Golly, B., Besombes, J.-L., Jaffrezo, J.-L., and Leoz-Garziandia, E.: Source apportionment of PM10 in an urban site using a PMF model applied on inorganic and organic chemical species. Atmos. Chem. Phys., 14, 3325-3346, 2014.

Xu, L., Guo, H., Boyd, C. M., Klein, M., Bougiatioti, A., Cerully, K. M., Hite, J. R., Isaacman-VanWertz, G., Kreisberg, N. M., Knote, C., Olson, K., Koss, A., Goldstein, A. H., Hering, S. V., de Gouw, J., Baumann, K., Lee, S.-H., Nenes, A., Weber, R. J., and Ng, N. L.: Effects of anthropogenic emissions on aerosol formation from isoprene and monoterpenes in the southeastern United States, Proceedings of the National Academy of Sciences, 112, 37-42, 10.1073/pnas.1417609112, 2015.

Xu, L., Williams, L. R., Young, D. E., Allan, J. D., Coe, H., Massoli, P., Fortner, E., Chhabra, P., Herndon, S., Brooks, W. A., Jayne, J. T., Worsnop, D. R., Aiken, A. C., Liu, S., Gorkowski, K., Dubey, M. K., Fleming, Z. L., Visser, S., Prévôt, A. S. H., and Ng, N. L.:

Wintertime aerosol chemical composition, volatility, and spatial variability in the greater London area, Atmos. Chem. Phys., 16, 1139-1160, 10.5194/acp-16-1139-2016, 2016.

Zhang, Q., Jimenez, J. L., Canagaratna, M. R., Ulbrich, I. M., Ng, N. L., Worsnop, D. R., and Sun Y.: Understanding atmospheric organic aerosols via factor analysis of aerosol mass spectrometry: a review. Anal Bioanal. Chem., 401, 3045-3067, 2011.

Zotter, P., Ciobanu, V. G., Zhang, Y. L., El Haddad, I., Macchia, M., Daellenbach, K. R., Salazar, G. A., Huang, R.-J., Wacker, L., Hueglin, C., Piazzalunga, A., Fermo, P., Schwikowski, M., Baltensperger, U., Szidat, S., and Prévôt, A. S. H.: Radiocarbon analysis of elemental and organic carbon in Switzerland during winter-smog episodes from 2008 to 2012 – Part 1: Source apportionment and spatial variability, Atmos. Chem. Phys., 14, 13551–13570, doi:10.5194/acp-14-13551-2014, 2014.

Figures main text

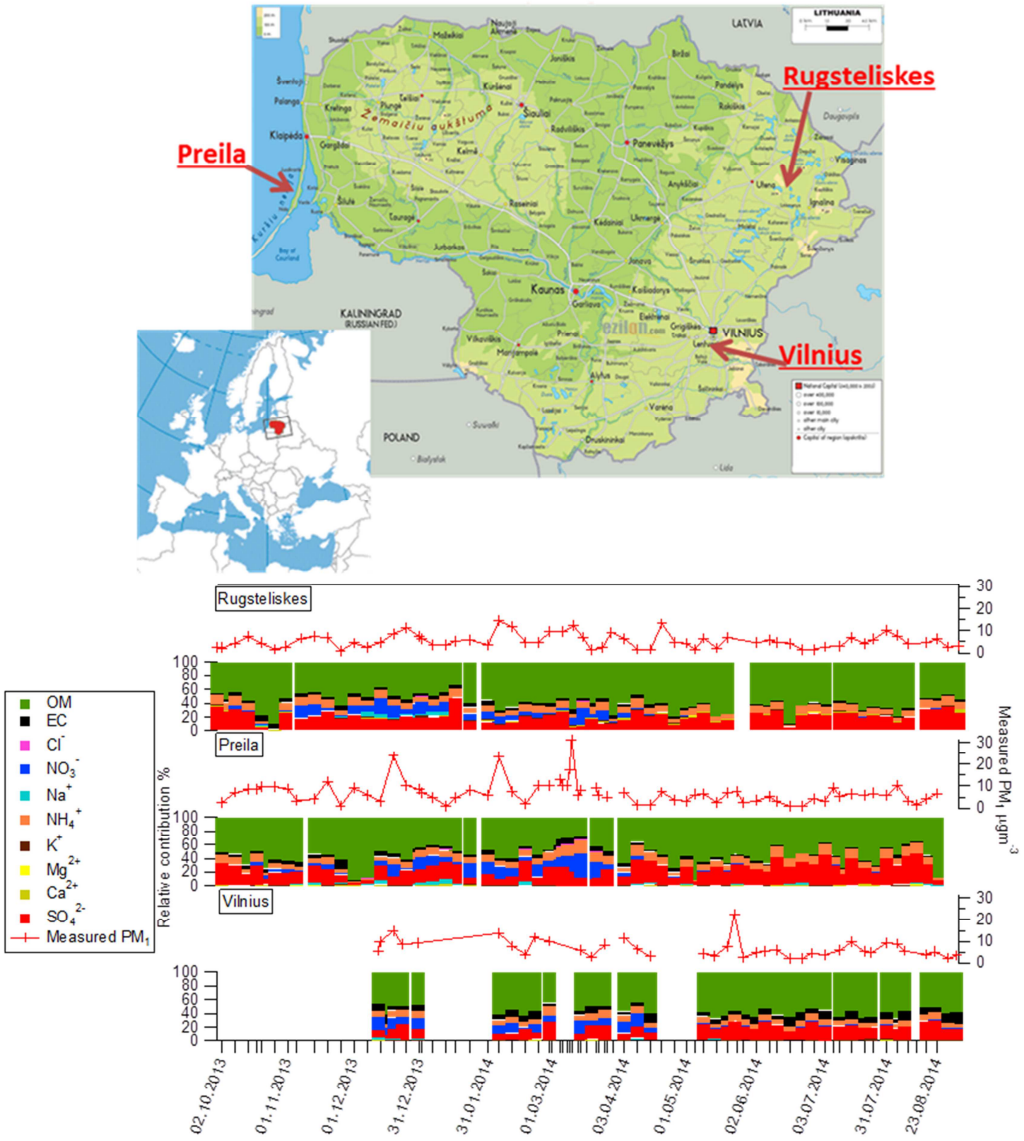

Figure 1. Sampling locations, and measured PM_1 composition. Ion concentrations from IC.

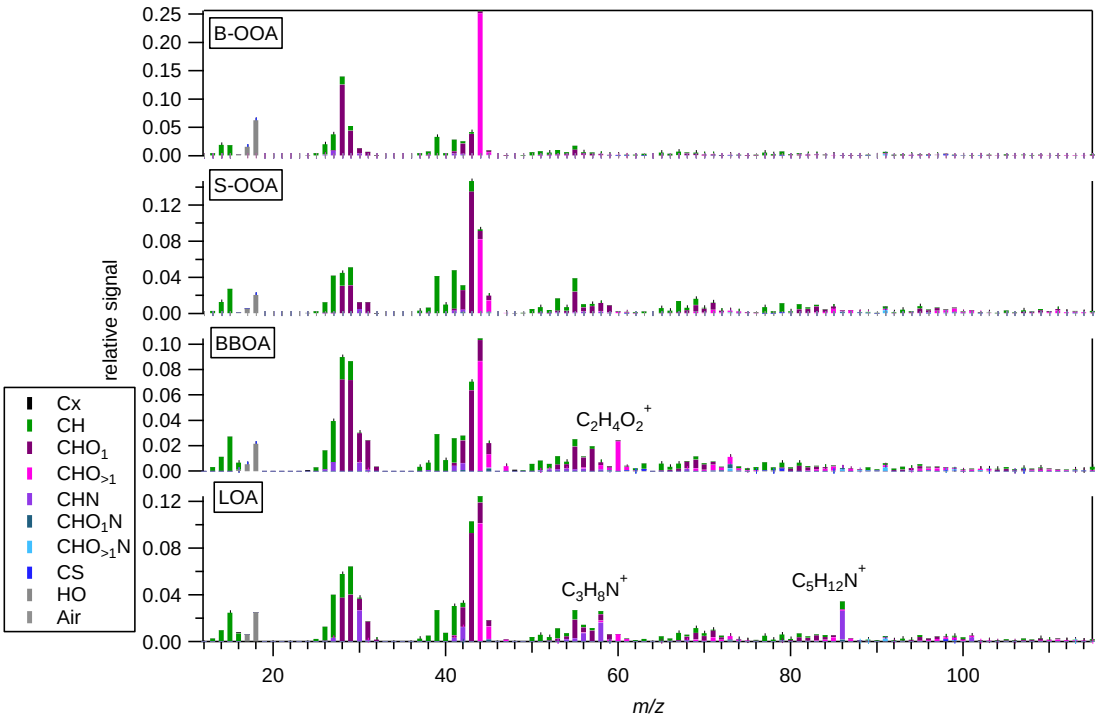

Figure 2. Offline-AMS PMF factor profiles: background oxygenated OA (B-OOA), summer oxygenated OA (S-OOA), biomass burning OA (BBOA), local OA (LOA).

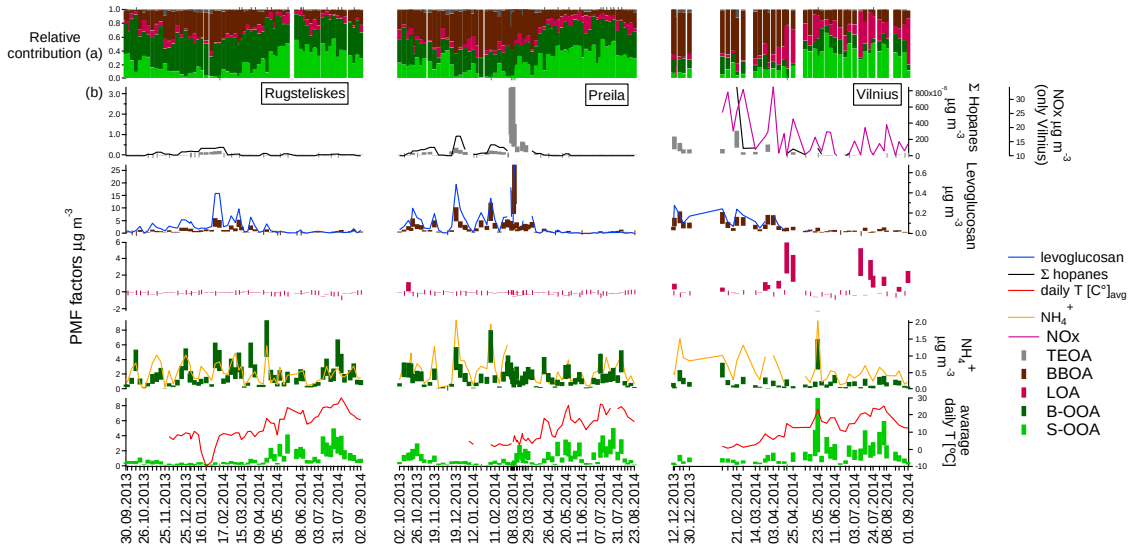

Figure 3. a) Temporal evolutions of relative contributions to the OA factors; b) OA sources and corresponding tracers: concentrations and uncertainties (shaded areas).

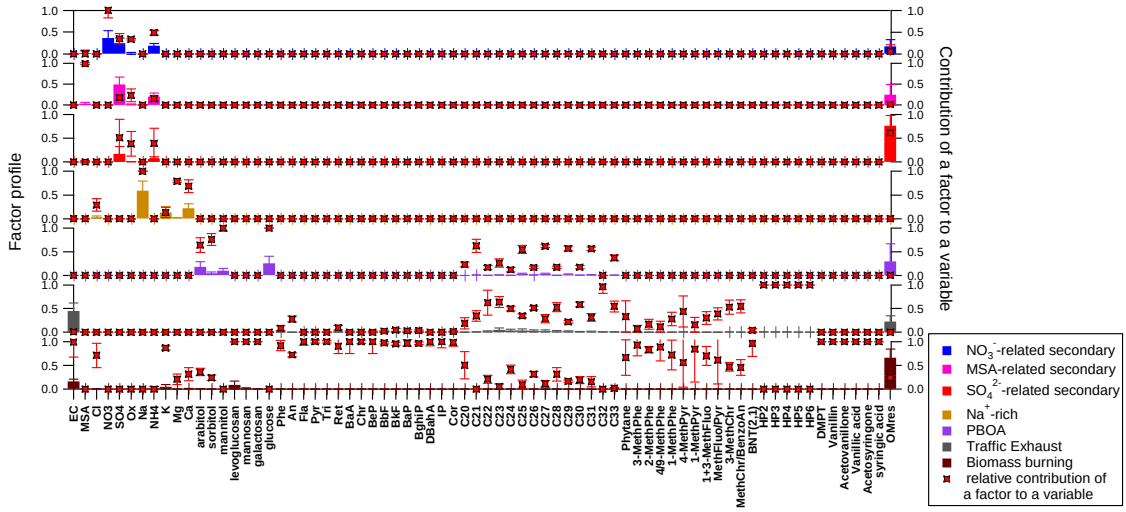

Figure 4. Marker-PMF factor profiles (bars) and relative contributions of the factors to the measured variables (symbols). Factor list and abbreviations: NO_3^--related secondary aerosol (NO_3^-related SA), SO_4^{2-}-related-SA, MSA-related-SA, Na^+-rich aerosol, primarybiological organic aerosol (PBOA), traffic exhaust (TE), biomass burning (BB).

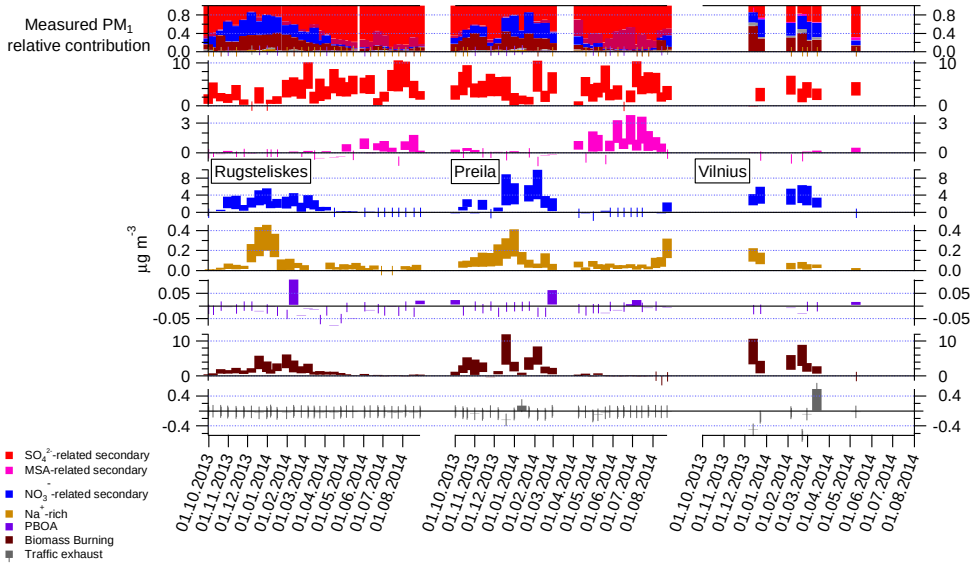

Figure 5. PM_1 marker source apportionment: factor time series and relative contributions. Shaded areas indicate uncertainties (standard deviation) of 20 bootstrap runs.

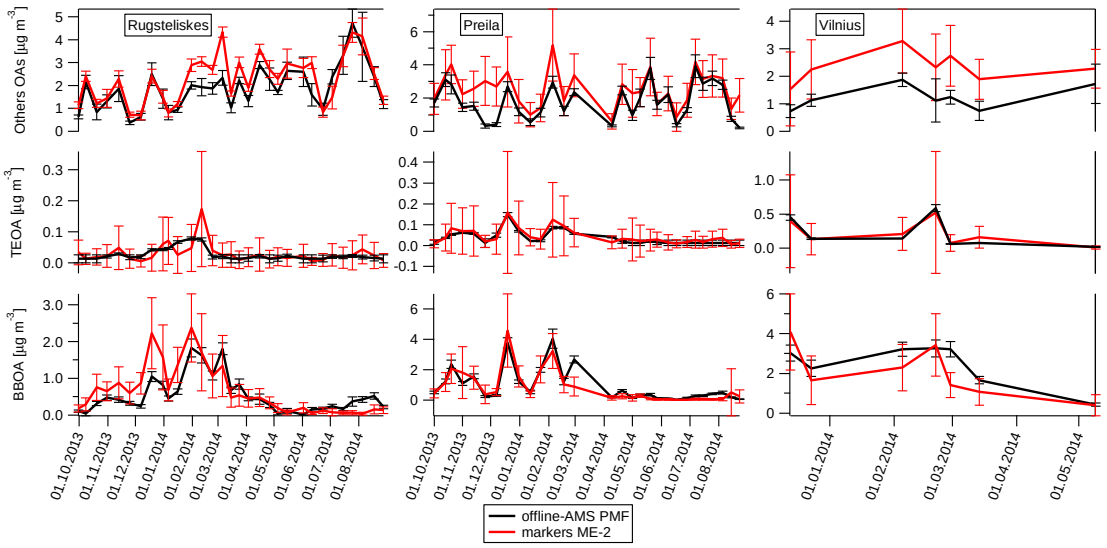

Figure 6. Marker-PMF and offline-AMS OM source apportionment comparison.

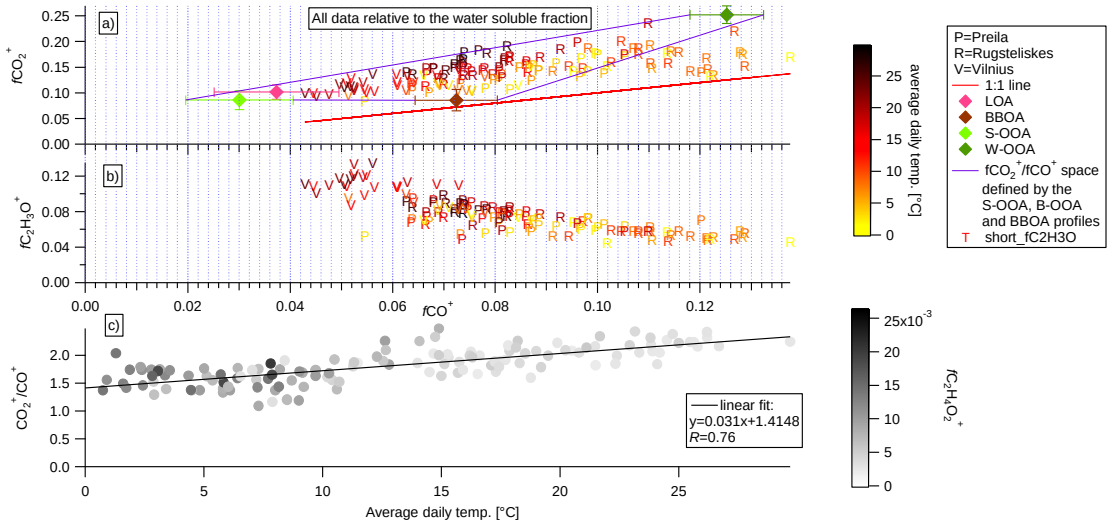

Figure 7. a) water-soluble fCO_2^+ vs fCO^+ scatter plot. Color code denotes the average daily temperature [°C], diamonds indicate the fCO_2^+/fCO^+ ratio for different PMF factor profiles. The 1:1 line is displayed in red. Few points from Rūgšteliškis lie outside the triangle, suggesting they are not well explained by our PMF model. However, Fig. S5 displays flat residuals for Rūgšteliškis, indicating an overall good WSOM explained variability by the model. b) water-soluble $fC_2H_3O^+$ vs fCO^+ scatter plot. Color code denotes the average daily temperature [°C] c) Scatter plot of the water-soluble CO^{2+} to CO^+ ratio *vs.* average daily temperature. Grey code denotes $fC_2H_4O_2^+$.

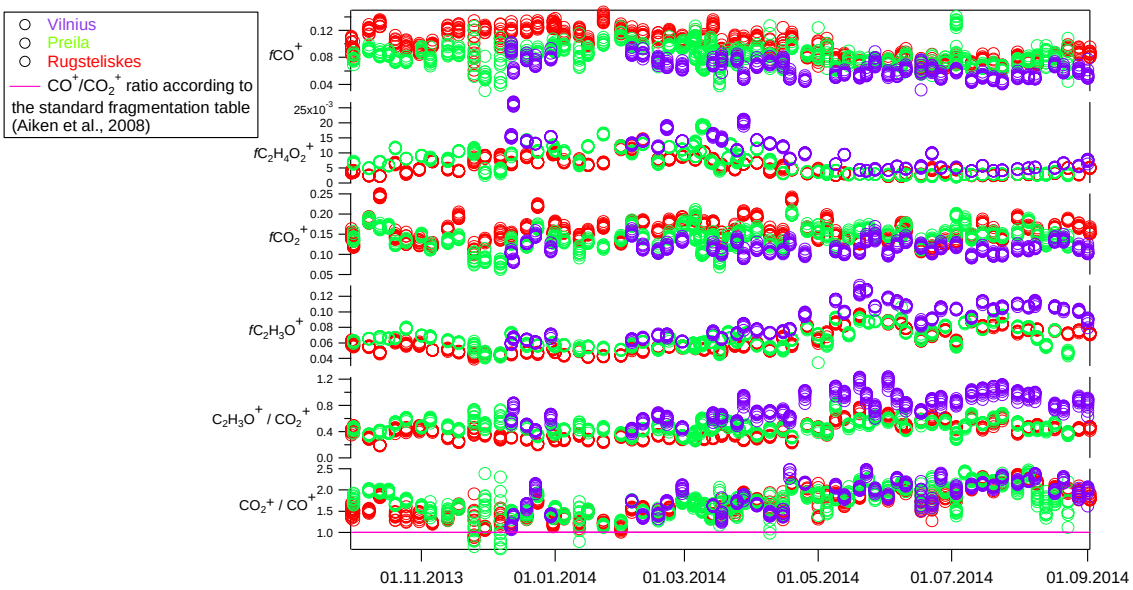

Figure 8. Time-dependent fractional contributions (*f*) of typical AMS tracers.